GEOFLUIDS
Geofluids (2014) **14**, 459–480 doi: 10.1111/gfl.12088

# Red calcite: an indicator of paleo-karst systems associated with bauxitic unconformities

O. GYŐRI[1,2], R. ORBÁN[1,*], A. MINDSZENTY[1], L. FODOR[2], Zs. POROS[2,†], A. ERŐSS[1], Zs. BENKÓ[3] AND F. MOLNÁR[1,‡]

*[1]Eötvös Loránd University, Budapest, Hungary; [2]MTA-ELTE Geological, Geophysical and Space Science Research Group, Budapest, Hungary; [3]Institute of Nuclear Research of the Hungarian Academy of Sciences, Debrecen, Hungary *MOL Plc. Exploration & Production Exploration Laboratories, H-1039 Batthyány street 45, Budapest, Hungary; [†]ConocoPhillips, 600 N Dairy Ashford, 77079, Houston, TX, USA; [‡]Geological Survey of Finland, PO Box 96, FI-02151, Espoo, Finland*

## ABSTRACT

A unique red calcite generation, which fills fractures/cavities, is hosted by Mesozoic carbonates in the Transdanubian Range, Hungary. Solid inclusions are located along growth zones of calcite. Hematite, the most abundant solid inclusion, gives the red colour of it. Outcrop-scale geometry, mineralogical features and detrital mineral assemblage (hematite, gibbsite, goethite, kaolinite, smectite, illite, Cr-spinel, monazite, xenotime, zircon, apatite and Ti-oxide) of calcite precipitates suggest strong correlation between the calcite and nearby karst bauxite deposits. Fluid inclusion petrography and microthermometry ($T < 50$°C; salinity from 0 to 0.17 NaCl eq. w%) of primary fluid inclusions, and the stable isotope trend of the calcite, following the meteoric water line, clearly indicate vadose and phreatic meteoric origin in a near-surface karst system. The late Cretaceous to mid-Eocene unconformity-related cavity-filling deposits occur close to the surface; indicating that the most recent Quaternary exhumation re-exposed those surfaces that existed at the time of calcite mineralization. Thus, red calcite precipitates are interpreted as being speleothems, vestiges of the subterranean part of the pre-Middle Eocene karst. The infiltrated, fine bauxite particles enclosed by the calcite are the witnesses of the once areally extensive pre-Middle Eocene bauxitic blanket that became partially eroded by the time of the deposition of the cover beds. Red calcite when found in core samples may provide good evidence on bauxite formation associated with the overlying unconformity, even if it was later removed by erosion. Therefore, presence or absence of red calcite may be used as distinguishing criteria between karst episodes with or without bauxite formation.

Key words: carbonate diagenesis, fluid inclusions, karst bauxite, paleokarst, red calcite, speleothem, stable isotopes, Transdanubian Range

Received 4 December 2013; accepted 15 May 2014

Corresponding author: Orsolya Győri, MTA-ELTE Geological, Geophysical and Space Science Research Group, H-1117, Hungary.
Email: gyori.orsi@gmail.com. Tel: +36 1 372 2500, ext. 1782. Fax: +36 1 381 2128.

*Geofluids* (2014) **14**, 459–480

## INTRODUCTION

Understanding the origin and spatial distribution of fissure/cavity-cementing minerals hosted by sedimentary rocks provides a key to reconstruct paleo-fluid flow systems. Precipitation of fracture-filling cement minerals in sedimentary rocks may be the result of volcanism-related hydrothermal fluid circulation (Thompson 1995). Other process leading to mineralization may be tectonic deformation and deformation-induced fluid motion (Machel & Cavell 1999). Fluids, released from the buried sediments due to compaction represent another type of mineralizing fluid-flow (Moore 1989; Deming *et al.* 1990). Finally, mineralization can be related also to surface exposure, alteration (dissolution and weathering) of rocks, and precipitation of minerals from near-surface (meteoric) fluids (James & Choquette 1988; Bosák *et al.* 1989). The latter can be particularly pronounced when carbonate rocks are affected by karstification. Surface exposure is generally recorded by important hiatuses in the sedimentary record.

Unconformity-related mineralization plays an important role in understanding the geological evolution of any given area, since it frequently represents the only record of a longer period otherwise not preserved as a stratified sedimentary sequence or as an igneous unit. It holds information about physical conditions of paleo-fluid flow and may contain petrographic or geochemical information, which are connected to the paleomorphology and paleoclimate of the given area.

In this article, we present a case study of a red, coarse-crystalline calcite mineralization filling numerous fractures and cavities in Mesozoic carbonates of the Transdanubian Range (TR), central Hungary. Despite the widespread studies on these red calcite 'dykes' from petrological, geochemical and structural geological points of view (Taeger 1909; Balásházy 1979; Tóth & Tóth-Gecse 1981; Gatter 1984; Demény 1992; Demény *et al.* 1997; Kercsmár 2004; Pálfalvi *et al.* 2006; Gál-Sólymos *et al.* 2008), their age and origin still remain ambiguous. As to the genesis of the red calcite veins, most of the above cited papers suggest a mixed magmatic-hydrothermal-meteoric origin, based on the apparently relatively high temperature of the parent fluid (homogenization temperatures of the primary fluid inclusions are ranging between approximately 100 to 180°C), the hydrothermal-meteoric mixed stable isotope values and the relatively high-temperature exotic mineral assemblage (such as monazite, xenotime, etc.) associated to them (Gatter 1984; Demény 1992; Demény *et al.* 1997). Most of them assigned the formation of the red calcite dykes to the Late Cretaceous lamprophyre magmatism (Horváth *et al.* 1983; Horváth & Ódor 1984; Szabó *et al.* 1993; Gyalog & Horváth 2004). However, none of these studies could explain the apparent lack of spatial correlation between calcite occurrences, widely distributed throughout the TR, and the Cretaceous magmatic rocks, limited to a smaller area within the TR.

Detailed studies focussing on red calcite outside Hungary are absent and occurrences are rarely mentioned in the international literature (Goldstein 1990; Palmer & Palmer 2008; Košir *et al.* 2013). The objective of this study is to establish the origin and nature of the fluid from which the red calcite precipitated, by studying the calcite and the host rocks in the field supplemented by petrography and numerous analytical methods.

## GEOLOGICAL SETTING

Five representative localities were selected for detailed study (Fig. 1). All the studied quarries are located of central-western Hungary (Fig. 1). TR is made up of slightly metamorphosed Lower Paleozoic rocks and overlying nonmetamorphosed Permo-Mesozoic and Cenozoic sediments (Fig. 2). Initially, it was part of the passive margins of both the Triassic-Jurassic Neotethys and Jurassic Alpine Tethys (Schmid *et al.* 2008). In consequence, it is characterized by thick succession of Mesozoic carbonates. Based on facies analogues, at that time this unit was supposedly situated somewhere between the depositional environments of the present Southern Alps and Northern Calcareous Alps (Kázmér & Kovács 1985; Haas *et al.* 1995). During the Cenozoic, it shared an eastward extrusion motion with other units, as part of the first-order AlCaPa composite unit (Kázmér & Kovács 1985; Ratschbacher *et al.* 1991; Csontos *et al.* 1992; Tari 1994); the southern boundary of it would be the Mid-Hungarian Shear Zone.

Due to the continuous isostatic subsidence, cyclically organized carbonates were deposited from the late Early Triassic on. The opening of Neotethys reached the area in the Middle Triassic (Bertotti *et al.* 1993), when carbonate shelves were dissected and the basins became filled by marls and cherty limestones (Budai 1989; Haas *et al.* 1995; Gawlick *et al.* 1999). In the Late Triassic a large carbonate platform developed along the margins of the Neothetys Ocean. Multiple deformation events affected the TR in Late Jurassic times because of the gradual closing of Tethys. Folding and thrusting in the Early Cretaceous resulted in a foreland basin and in front of it, the development of a forebulge unconformity (Tari 1994; Mindszenty *et al.* 2001). Karst bauxite deposits formed on the exposed karst terrains (Combes & Bárdossy 1996; Mindszenty *et al.* 2001). The NE-SW trending synformal structure of the TR formed in mid-Cretaceous (Albian) times and controlled the facies distribution of the overlying sediments during the late Albian to Cenomanian but also during the Santonian. The late Cretaceous in the TR was characterized by marl deposition in the basins while rudist reefs were growing on the platform top and slopes (Haas 1983). The absence of latest Cretaceous (Maastrichtian), Paleocene and early Eocene sediments indicate another subaerial exposure phase, represented by the most widespread Eocene karst bauxite horizon. As the result of Albian, Santonian and Cretaceous to early Eocene exposure periods erosion reached the Upper Triassic carbonates also along the limbs of the major Transdanubian syncline. Repeated transgression episodes in the Middle and in the latest Eocene resulted in the deposition of shallow marine limestones and shallow bathyal marls (Báldi & Báldi-Beke 1985). From the late Early Oligocene on alluvial siliciclastics were deposited in the area (Korpás 1981). After an Early Miocene hiatus, shallow marine sedimentation occurred in the Middle Miocene. The range was uplifted during the late Pliocene to Quaternary (Tari 1994; Horváth & Cloetingh 1996), when eolian loess, fluvial gravels, slope deposits and travertines deposited in small thicknesses.

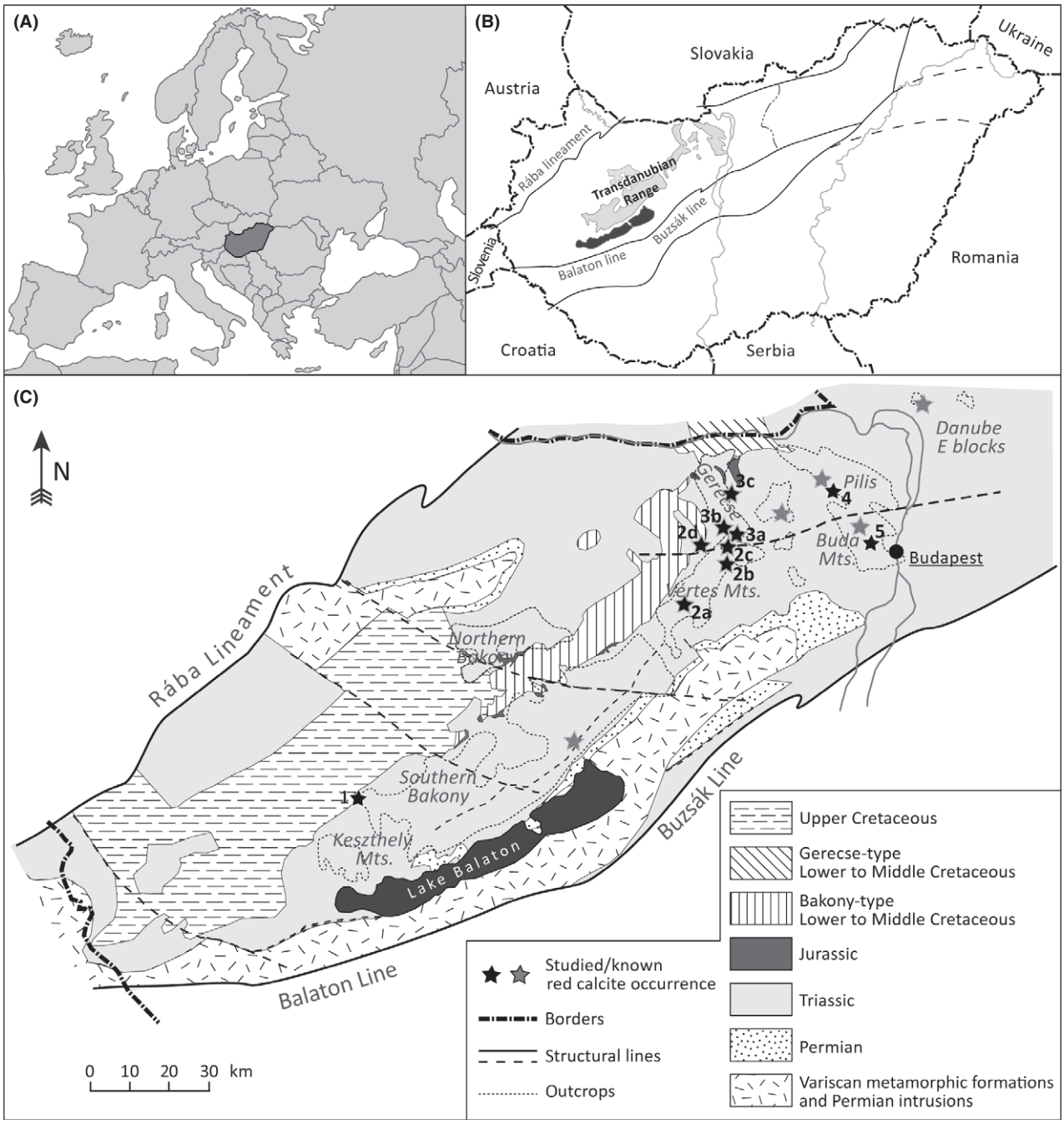


**Fig. 1.** (A) Location of Hungary in Europe (B) Main tectonic lineaments in Hungary and the position of the Transdanubian Range (TR) (C) Pre-Cenozoic geological map of the TR (modified after Haas *et al.* 2010 and Haas 2012). Studied outcrops are indicated by black stars. 1. Sintérlap Quarry (N 46°58′10″ and E 17°16′50″); 2. Vértes Hills: 2a Kápolnapuszta (N 47°24′31″ and E 18°19′55″), 2b Terv road (N 47°31′6″ and E 18°24′22″), 2c Zsidó Hill (N 47°30′43″ and E 18°24′32″), 2d Orosz-kút (N 47°30′50″ and E 18°23′53″); 3. Gerecse Mts.: 3a Tatabánya, Kálvária Hill (N 47°32′53″ and E 18°27′4″), 3b Tatabánya, Keselő Hill (N 47°33′46″ and E 18°27′14″), 3c Héreg (N 47°38′30″ and E 18°32′32″); 4. Pilisjászfalu Quarry (N 47°39′38″ and E 18°48′13″); 5. Hárs Hill Quarry (N 47°31′50″ and E 18°57′15″). Coordinates are given in WGS84 system.

## METHODS

Field structural measurements were carried out in several outcrops. Structural measurements are illustrated on stereographic projections, using the software of Angelier (1984). A total of 109 hand specimens were taken from the studied outcrops for petrographic and geochemical studies. Detailed petrography was carried out on 50 thin-sections, 30 μm-thick, prepared at the Department of Physical and Applied Geology, Eötvös Loránd University

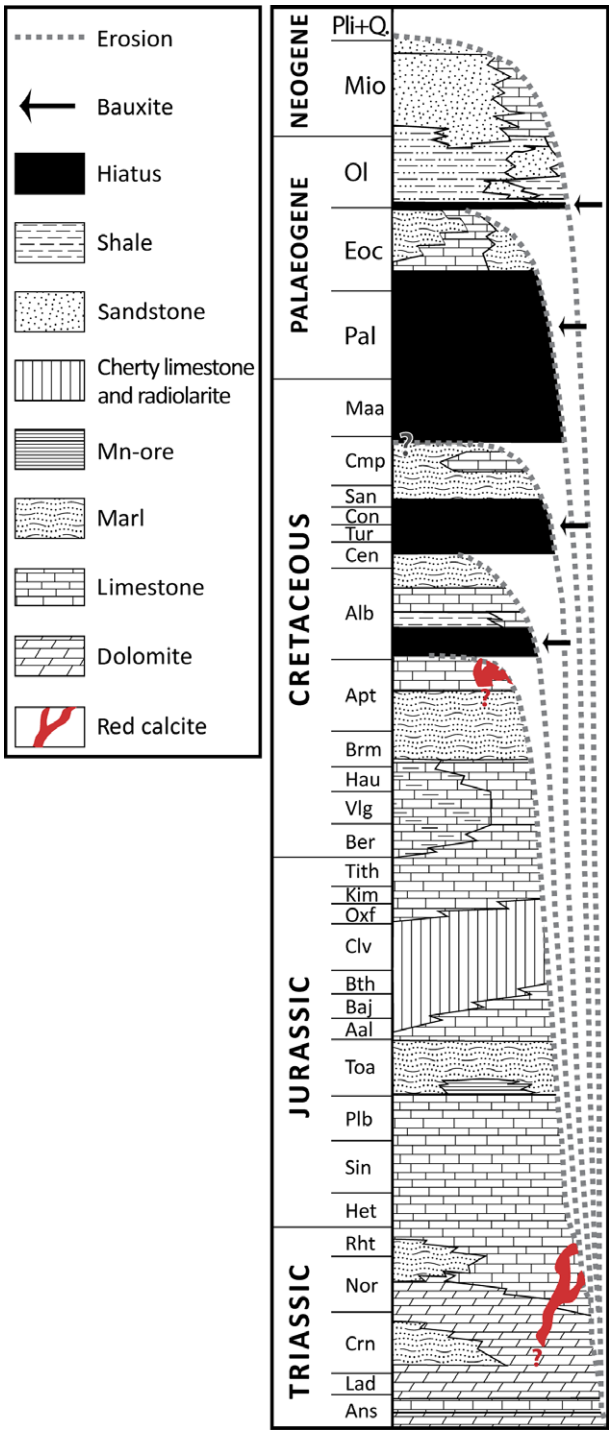


**Fig. 2.** Generalized stratigraphic column of the Transdanubian Range (modified after Mindszenty *et al.* 1991).

(ELU). A solution of alizarin red-S and potassium ferricyanide was used to identify the carbonate phases in the samples (Dickson 1966). Cathodoluminescence (CL) studies were performed using a MAAS-Nuclide ELM-3 cold-cathode Luminoscope (Measurement and Analysis Systems, Inc., Lowell, MA, US) at the Department of Physical and Applied Geology, ELU.

Doubly polished thin-sections, 100 μm-thick, were prepared for fluid inclusion studies, avoiding the heating of the samples. Microthermometry of the fluid inclusions was performed on a Linkam FTIR heating-freezing stage (Linkam, Guildford, UK) at the Department of Mineralogy, ELU. Standardization has been carried out on −56.6, 0 and 385°C on natural and synthetic fluid inclusions. Accuracy of the measurements was 0.1°C during heating experiments and 1°C during freezing.

Stable carbon and oxygen isotope analysis was done in the Research Centre for Astronomy and Earth Sciences, Hungarian Academy of Sciences. Individual laminae of the calcite and other components of the studied samples were subsampled separately by using a drilling bit with a diameter size of 0.6 mm. The pulverized subsamples were treated by anhydrous phosphoric acid using continuous flow technique (Spötl & Vennemann 2003). The isotope ratios of the resulting equilibrated $CO_2$ gas was measured by a Finnigan MAT delta S type mass spectrometer (Thermo Fisher Scientific, Bath, UK). Standardization was conducted using laboratory calcite standards calibrated against the NBS 18 and NBS 19 standards. During the measurement of the dolomite samples a laboratory dolomite standard was used. Isotope compositions are expressed in δ notations as permil deviations from the V-PDB (Vienna Pee Dee Belemnite) carbonate standard. Reproducibility of $\delta^{18}O$ and $\delta^{13}C$ values is better than ±0.2 ‰.

To identify the solid inclusions, calcite samples were dissolved in 10% hydrochloric acid. Heavy mineral separation was done on the dissolution residue of the calcite samples. X-ray powder diffraction (XRPD) measurements were carried out on the dissolution residue by a Siemens D 5000 type diffractometer at the Department of Mineralogy, ELU. The XRPD data was evaluated by DIFFRAC$^{plus}$ EVA program. Scanning electron microscopic investigations were done with an Amray 1830i instrument (Amray, Bedford, MA, USA) equipped with INCA Energy-dispersive X-ray spectrometer (EDS) at the Department of Petrology, ELU.

## RESULTS

### Field observations

Red calcite, filling fractures and cavities most commonly hosted by Triassic and Cretaceous carbonate rocks, occurs at several localities within the TR. The following outcrops were chosen for detailed investigation (Fig. 1): Sintérlap Quarry at Sümeg (site 1), Vértes Hills (sites 2a, 2b, 2c and 2d), Kálvária Hill and Keselő Hill near Tatabánya (site 3a, 3b), Héreg in the Gerecse Mts. (site 3c), Pilisjászfalu Quarry (site 4) and Hárs Hill (site 5) near Budapest.

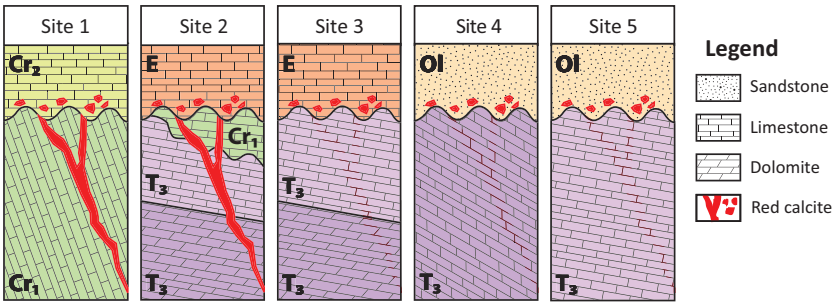


**Fig. 3.** Cartoon showing the stratigraphic relationship between red calcite, host rocks, and the overlying sedimentary rocks at the five studied localities.

### Stratigraphical position of the red calcite

The strongly tilted (folded) and imbricated Lower Cretaceous (Aptian) shallow-marine limestone hosts red calcite veins at site 1 (Figs 1, 3 and 4A). Reworked clasts of the red calcite veins can be found in the overlying Campanian platform limestone suggesting pre-Campanian age for the calcite formation at this location (Haas *et al.* 1985). At site 2, red calcite filled fractures are hosted by Upper Triassic platform carbonates (Hauptdolomit and Dachstein Limestone), and Lower Cretaceous (Aptian to earliest Albian) shallow-marine limestone (Budai *et al.* 2008; Fodor *et al.* 2008). At site 3b both the upper and lower quarries expose red calcite hosted by Upper Triassic platform carbonates (Figs 3 and 4B). Dip of the beds is approximately 30° NW. The Upper Triassic is exposed here in almost 70 m thickness, below the major Eocene unconformity. Reworked fragments of the red calcite were found embedded in the Middle Eocene shallow-marine limestone, unconformably overlying the Triassic carbonates at site 3b (Kercsmár 2008). A red calcite filled cavity is cut by the basal Eocene unconformity and covered by Middle Eocene limestone at site 3a (Fig. 4C). At the north-eastern part of TR, site 4 (Fig. 1) exposes moderately dipping beds of Triassic dolomite, hosting red calcite (Fig. 3). Some cm-sized fragments of red calcite can be found in the Oligocene shallow-marine sandstone, which unconformably overlies the Triassic dolomite (Sásdi 2000). This sandstone was also found covering the surface of red calcite in fractures and cavities (Fig. 4D). At site 5 (Fig. 1), the red calcite-hosting Triassic limestone is overlain by Eocene and Oligocene sediments (Fig. 3).

### Red calcite filled fractures and cavities

Red calcite filled structures have two major types of geometry. Calcite fills 10–100 cm-wide fractures of 1–15 m length (i). The fracture planes are relatively planar. Mapping revealed that the longest red calcite vein could be traced for 200 m at site 2, either as a single body or several smaller bodies aligned along strike (Fodor *et al.* 2008). Calcite and the related sediments also fill up to 1 m-wide, isometric cavities in the carbonate rocks (ii) (Fig. 4B,E). Most fractures and all cavities are completely filled by the calcite (Fig. 4E), but some of the fractures still have some remaining pore space, commonly filled by yellow to grey marl. Width and strike of the veins are highly variable.

The red calcite filled cavities are either isometric or vertically elongate. At sites 3b and 4 some of the cavities are completely filled with red coarse-crystalline (1–20 cm) calcite (Fig. 4E), while the others are partially filled by red laminated sediments at the bottom and with white to red calcite in the remaining pore space. The red micritic sediments are also completely cemented by calcite. The Triassic limestone, hosting the cavities at site 5, is highly porous. The surface of the red calcite is commonly corroded.

At site 3b 2 m-high and 1.5 m-wide structures were exposed, all of which are made up by red calcite, showing flowstone morphology (Fig. 4F). Red calcite, filling either partially or completely a fracture, exhibits laminated structure, delineated by colour zonation. Enrichment in solid inclusions typifies the red zones. Some zones are so rich in this detrital material, that they are rather considered to be fine-grained sediment, cemented by red calcite (Fig. 5A). Similar fine-grained, calcite-cemented sediments also occur in several localities at site 2 (Fodor 2008). Some fractures that are only partially cemented by flowstone are also filled by yellow-grey laminated marl. At site 3a, red calcite cements pre-existing fractures of various orientations. The red calcite was occasionally precipitated on striae of this earlier deformation phase, clearly indicating the relative timing of faulting and mineralization. Both the faults and calcites are truncated at the basal mid-Eocene breccia or limestone layers (Fig. 4C, Kercsmár 1995). At site 3a, red calcite dripstone occurs in a cavity of ca. 1 m in diameter (Fig. 5B). The remaining space was filled by fossiliferous marly carbonate sediment. The fauna is typical for the overlying Middle Eocene shallow-marine limestone (Kercsmár 1995).

The calcite usually forms several cm-thick laminated crusts delineated by white-transparent and red zones (Fig. 5C,D), but it also occurs as coarse-crystalline calcite in several shades of brown, red and yellow. The columnar calcite crystals are always perpendicular to the substrate. A 40 cm-wide fissure was found at site 3b, filled by pink calcite on the wall and coarse-crystalline white calcite in the middle (Fig. 5E).

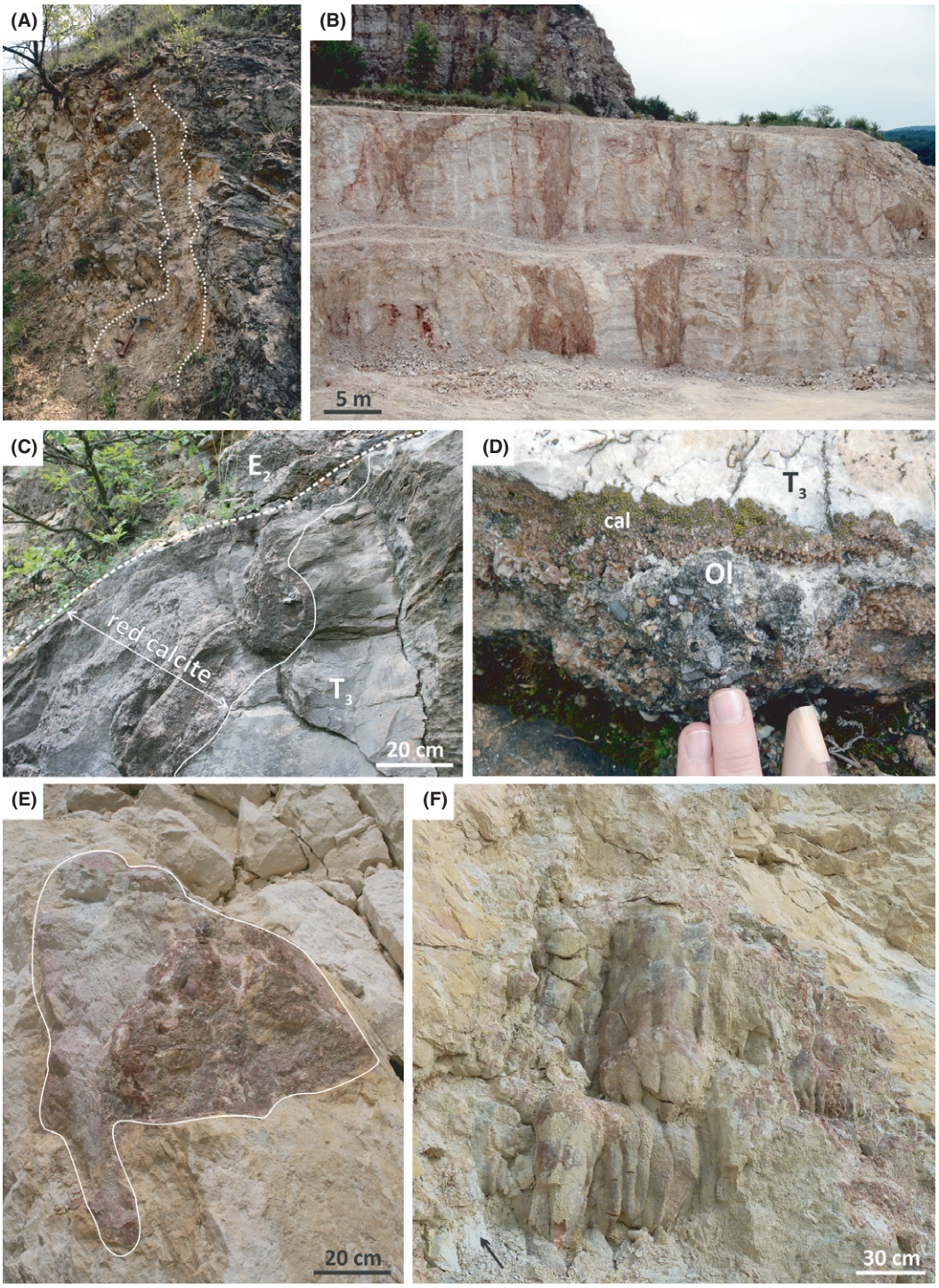


**Fig. 4.** (A) Red calcite cementing a dissolution-enlarged fracture that crosscuts the Lower Cretaceous shallow-marine limestone at site 1; (B) Red calcite fills fractures hosted by the Upper Triassic dolomite, site 3b; (C) Red calcite cavity-fill hosted by the Upper Triassic dolomite, in erosional contact (dashed line) with the Middle Eocene basal breccia, site 3a; (D) Oligocene sandstone filling the remaining space in a fracture, previously partially filled by red calcite, site 4; (E) Red calcite filled cavity in the Upper Triassic dolomite, site 3b; (F) Red calcite flowstone on the surface of the Upper Triassic dolomite, black arrow marks the grey laminated marl, deposited on the surface of the flowstone, site 3b.

### Contact of the red calcite and host dolomite

Where the red calcite veins are hosted by the Upper Triassic dolomite (at sites 3b and 4) 0.5–5 cm-wide zone was observed in the host dolomite, next to the red calcite veins, along which the otherwise yellow colour of the rock is faded (Fig. 5E). This phenomenon is very common also around the breccia filled cavities (Fig. 5C). The boundary of the veins towards the host rock is very sharp and irregular in each locality, irrespective of host rock (Fig. 4D). The irregularity of the boundary indicates that the fractures were enlarged by dissolution.

### Calcite-cemented breccia and claystone

Breccias were found at sites 3b, 3c and 4. The limestone/dolomite angular breccia clasts are floating in a calcite cemented red silt, completely occluding 10–80 cm-wide, irregular-shaped cavities in the host rock (Fig. 5F). The size distribution of the fragments is polymodal (Fig. 5F). The fragments are angular, and of 1–5 cm-size representing the host Triassic carbonate. One of these breccias is cross-cut by a 5 cm-wide red calcite vein (Fig. 5G). Similar breccia was also found at site 2c, forming a bed. The breccia is clast-supported in this case; with calcite-cemented red silt in-between the carbonate clasts.

Red claystone, usually also cemented by calcite was found on Triassic carbonate host rocks at sites 3b and 4 (Fig. 5H). Rarely, also black, carbonaceous silt was observed along red calcite filled fractures.

### Structural observations on the red calcite filled fractures

Walls of the fractures that host red calcite are either planar or, more commonly, undulating. They are of variable orientation. NW–SE striking fractures are common, especially at sites 2a, 3a and 3c (Fig. 6). Parts of these fractures were mapped for several hundred metres at site 2a (Budai *et al.* 2008). Another set is trending approximately N–S (sites 2a, 2d). It was also observed, at two sites (1, 3b), that red calcite fills NNE–SSW to NE–SW oriented fractures.

### Post-red calcite veins

Red calcite filled fractures and cavities are cross-cut by abundant, few cm-wide, transparent and yellow calcite veins at sites 3a, 3b, 4 and 5. As opposed to the red calcite veins, these latter veins, sometimes associated with barite could be also traced in the overlying rocks (such as the Eocene limestone and Oligocene sandstone). Therefore, it is possible to distinguish them from the solid inclusion-free, white version of the red calcites. Few mm-wide limonitic encrustation borders the calcite-barite veins. This paragenesis often occurs along reactivated red calcite veins. The stratigraphic position of these calcites shows, that they probably represent a younger fluid system, therefore they are not discussed in details in this paper.

## Petrography of the red calcite

On the microscopic scale, red calcite samples show diverse fabric. For the description of these microfabrics the terminology of Frisia and Borsato's system was used (Frisia & Borsato 2010).

Typical microfabric of the calcite from the investigated quarries is columnar (L:W ratio approximately 6:1). Elongation of the crystals is perpendicular to the substrate (Fig. 7A,B). The width of the columnar crystals varies between 30 μm and 1 mm. As a subtype of columnar fabric microcrystalline calcite (distinguished by Frisia *et al.* 2000) was also found at site 1. In this case the boundaries of the columnar domains are irregular, serrated and often show patchy extinction (Fig. 7C). Subordinately acicular-fibrous microfabric was also observed at sites 3b and 4. Associated to acicular red calcite at site 3b concentric structures were observed in cross-section, drawn by red laminae, composed of solid inclusions (Fig. 7D).

Voids in-between the needle-like calcite crystals from site 4 were subsequently filled by transparent mosaic calcite (Fig. 7E). Few of the samples from site 3b exhibit microcrystalline fabric. These samples are usually full of hematite inclusions, giving an intense red colour even in thin section.

Twin lamellae are common in each sample from site 1 (Fig. 7C) and in some sample from sites 2 and 5. The width of the lamellae is 100–200 μm. Stylolite with amplitude of few mm was observed cross-cutting red calcite at site 3b.

None of the red calcite samples contain divalent iron as revealed by staining and by the uniformly nonluminescent pattern.

Angular, 100–1000 μm-sized fragments of the host rock and white calcite are cemented by microsparite, in which 50–300 μm-sized solid inclusion aggregates form peloid-like structures. The calcite clasts are graded in this red stained, calcite cemented sediment. Another type of the breccias is where angular 1 mm to 1 cm-large dolomite (and some calcite) clasts are floating in a coarse grained (approximately 100 μm) matrix. The latter is full of spheroidal goethite grains, with no visible internal structure, and it is cemented by red calcite (Fig. 7F). Breccia from site 2 contains limestone clasts embedded in calcite-cemented red silt.

The faded, 0.5–5 cm-thick halo along the boundary of the calcite and the host dolomite is calcitic, as revealed by staining and SEM (Fig. 7G).

The yellow-grey marl, covering the surface of red calcite flowstone at site 3a, contains red algae, foraminifers, *Ostracod* shells and fragments of the calcite (Fig. 5B). Based on this bioclast assemblage the age of this sediment is most probably Eocene.

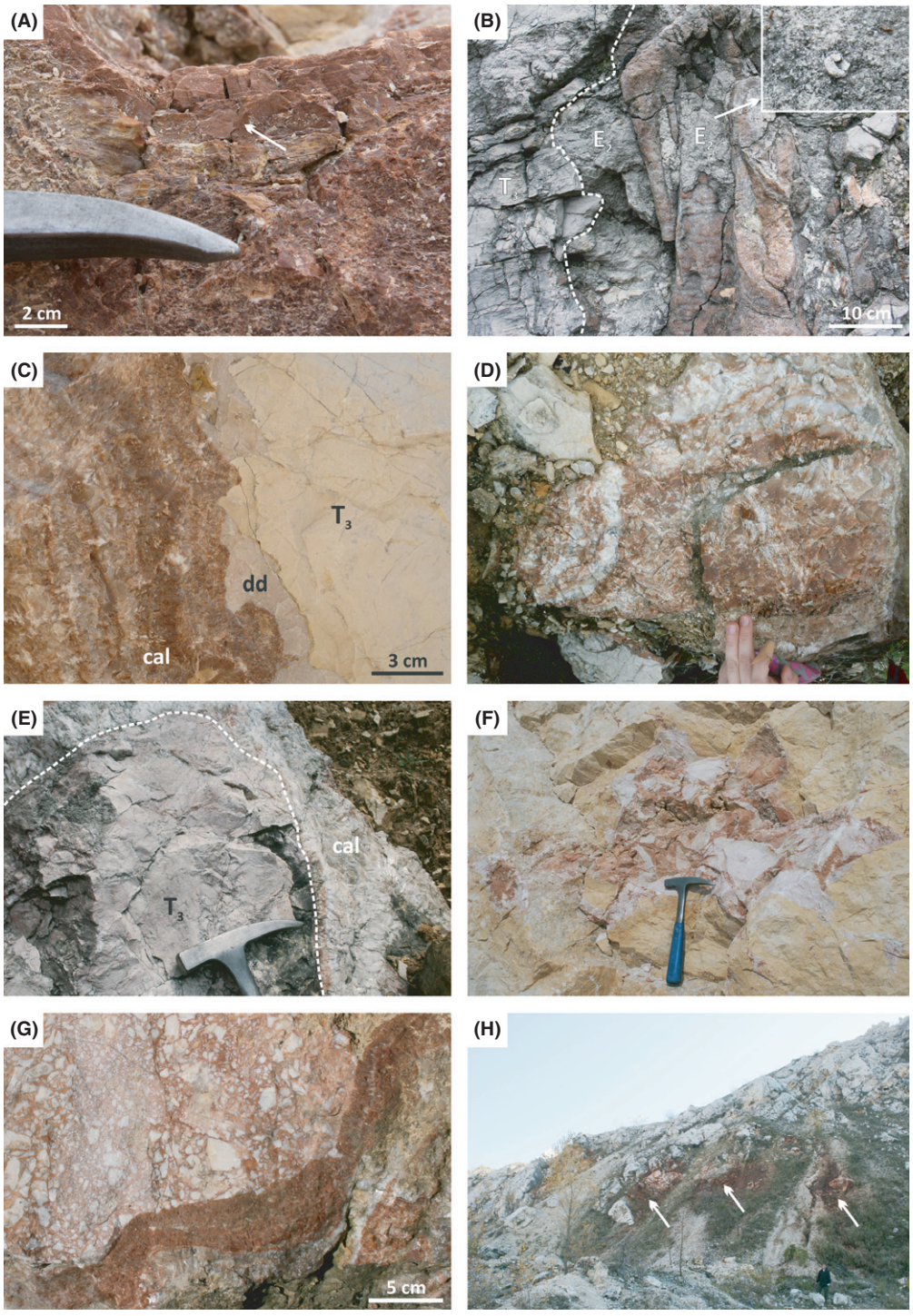


**Fig. 5.** (A) Solid inclusion-rich red calcite, site 3b; (B) Red calcite dripstone occurring in a cavity hosted by the Upper Triassic (T3) dolomite. Surface of the dripstone is covered by infiltrated fossiliferous sediment (E2). The fossil-content of it is very similar to that of the overlying Eocene limestone, site 3a; index picture shows fragment of an Echinoid; (C) Highly corroded boundary of a red calcite vein (rc) with a dedolomitized halo (dd) in the Upper Triassic dolomite (T3), site 3b; (D) White and red zones of coarse-crystalline calcite filling a cavity in Upper Triassic dolomite, site 4; (E) White calcite hosted by the Upper Triassic dolomite (T3), site 3b; (F) Dolomite clasts are floating in a red calcite-cemented matrix – collapse breccia structure from site 3b; (G) Red calcite cemented breccia in the Upper Triassic dolomite, crosscut by a red calcite vein, site 4; (H) Remnants of red silt on the Upper Triassic dolomite, marked by arrows, site 4.

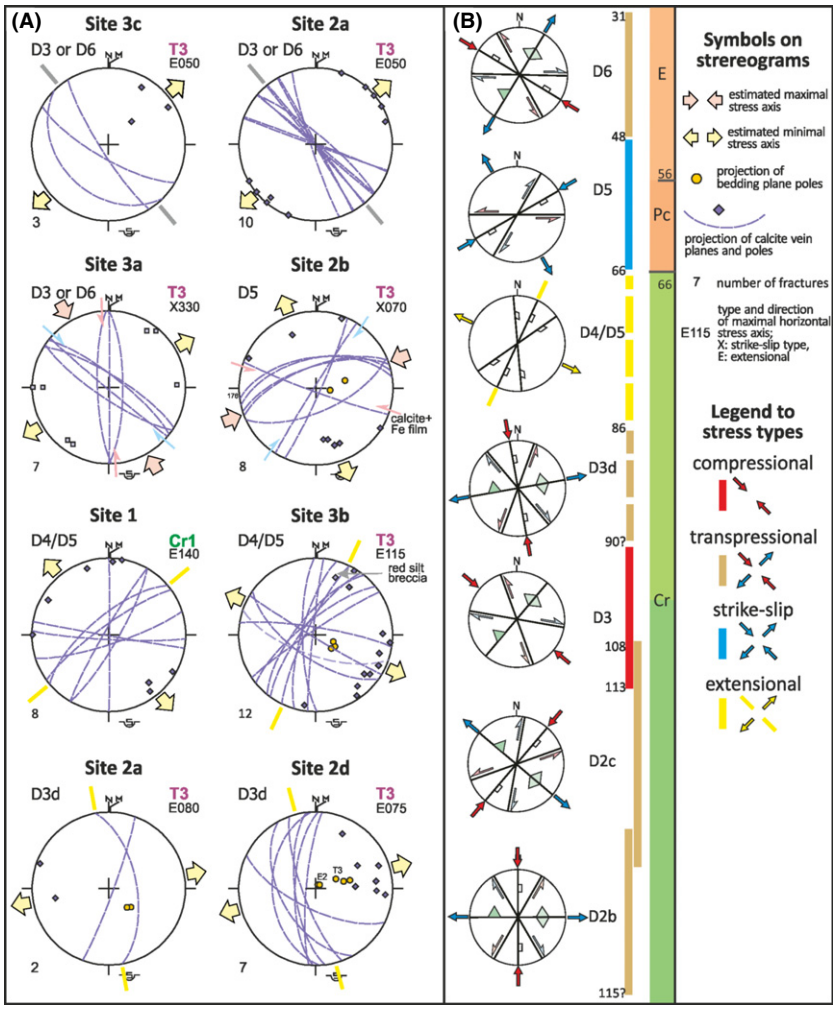


**Fig. 6.** (A) Stereograms, representing dip directions and dip angle of red calcite veins from different locations within the TR. (B) Simplified evolution of the fracture system and related stress field for the TR, between the Cretaceous and Eocene. Lower hemisphere projection, Schmidt net. Kinematics of the different sets is interpreted based on the tectonic evolution of the wider surroundings (Fodor 2008, 2010).

### Solid inclusions in the red calcite

The calcite is usually laminated and exhibits growth bands. Solid inclusions are concentrated in certain laminae (Fig. 7A). Spacing of the bands is 0.01–5 mm and they are parallel to each other. In some samples, like in the fibrous calcite samples from site 4, solid inclusions are evenly distributed. Small crystals, grown on the surface of solid-inclusion-rich bands, point to new nucleation. The solid inclusions are either 20–300 μm-sized individual crystals/grains or, more often they form 50–400 μm-sized aggregates. Size of the individual solid inclusions within these aggregates is around few μm as revealed by SEM. The XRPD results are presented on Fig. 8. Table 1 lists the detected solid inclusions for each locality.

HCl-insoluble residue of red calcite samples from sites 3b, 4 and 5 contains hematite, which gives the intense red to brown colour to the calcite. Goethite and lepidocrocite were also found. Clay minerals (illite, kaolinite, smectite) are present at each locality. Al-oxihydroxide and Al-hydroxide minerals, namely boehmite (sites 1, 3b and 4) and gibbsite (sites 3b, 4 and 5) were also detected in the samples from the studied localities. AlOOH (diaspore) was identified also by SEM in a sample from site 1 (Fig. 9A,B). Additionally some ilmenite, zircon, Cr-spinel, Mn-oxide, barite, mica, monazite, feldspar, plagioclase, epidote, amphibole, pyroxene, staurolite, garnet, pyrite, kyanite, dolomite, apatite and Ti-oxide were found in the dissolution residues. Quartz is present in each locality; however, it was extremely common in the samples from site 1.

### Fluid inclusion analysis

Primary aqueous inclusions in the red calcite samples of sites 1, 2, 3b and 4 are elongate and parallel to the c-axis of the crystal (*i.e.* parallel to the growth) (Fig. 10A,B), and commonly show a peculiar spike shape. The crystals are crosscut by curved, healed microfractures shown by secondary inclusions. Distribution of the primary inclusions is random within the individual crystals. The size of the inclusions varies between 5 to 150 μm, with the largest occurring in the samples from site 3b, while the smallest

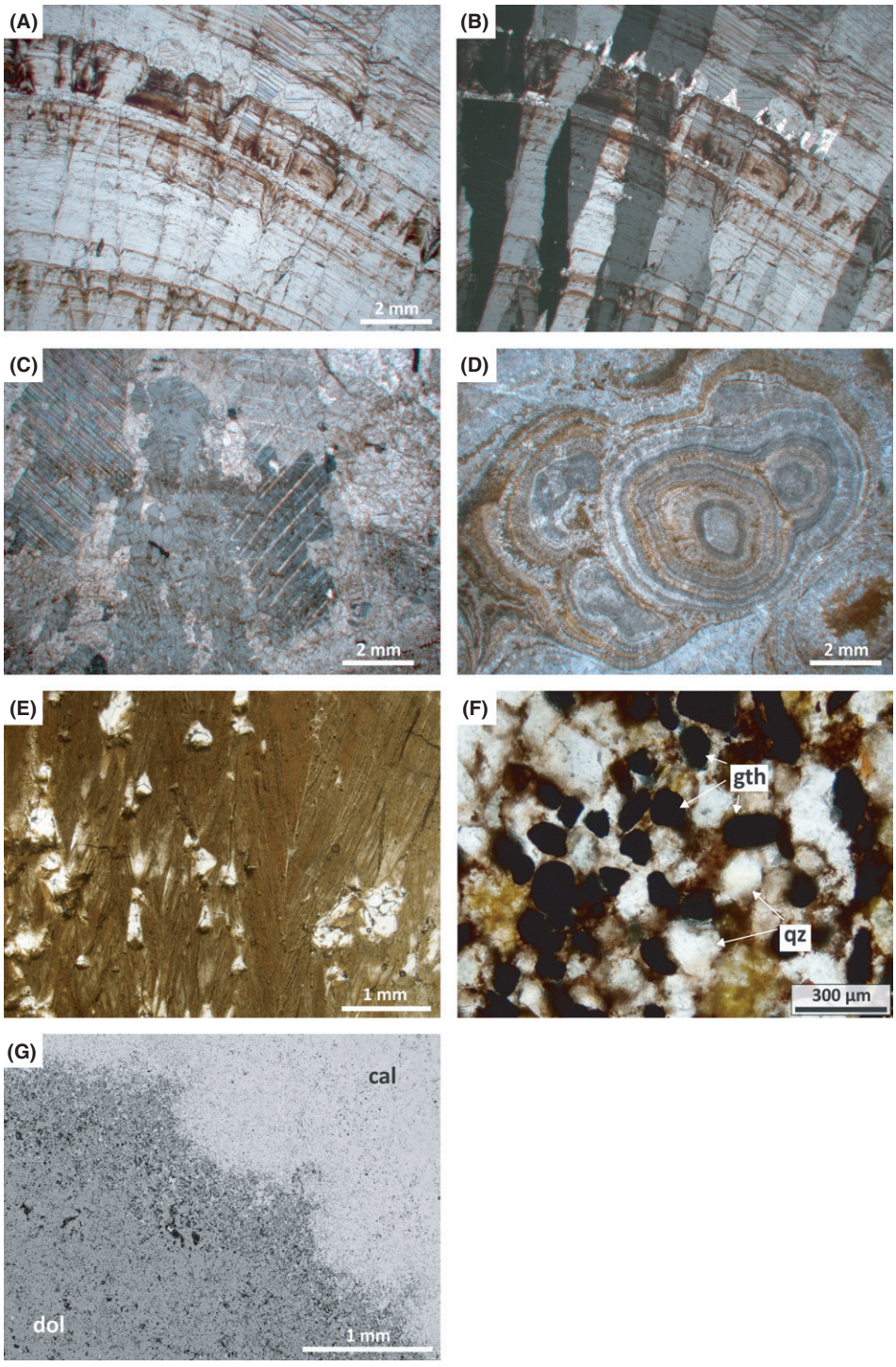


**Fig. 7.** (A) Red, solid inclusion rich laminae in calcite, site 1; (B) Columnar calcite crystals, same picture as (A) (crossed polars); (C) Patchy extinction pattern of twinned red calcite from site 1 (crossed polars); (D) Concentric structure in cross-section, drawn by solid inclusion-rich laminae in a red calcite sample from site 3b; (E) Fibrous, solid inclusion rich red calcite from site 4, voids in-between the needle-like calcite crystals were subsequently filled by transparent mosaic calcite; (F) Rounded goethite grains (gth) and some angular quartz grain (qz), cemented by red calcite (yellow to reddish brown cement in-between the grains), site 3b; (G) Gradual transition between the red calcite and the dolomite host rock on SEM-BSE image, sample from, site 3b.

were observed in the calcite from site 4. Laminated samples commonly contain fluid inclusions in the transparent (solid inclusion free) zones. Site 4 is the only one from the different localities, where primary fluid inclusions were possible to observe also in the solid inclusion rich zones of the crystal (Fig. 10C).

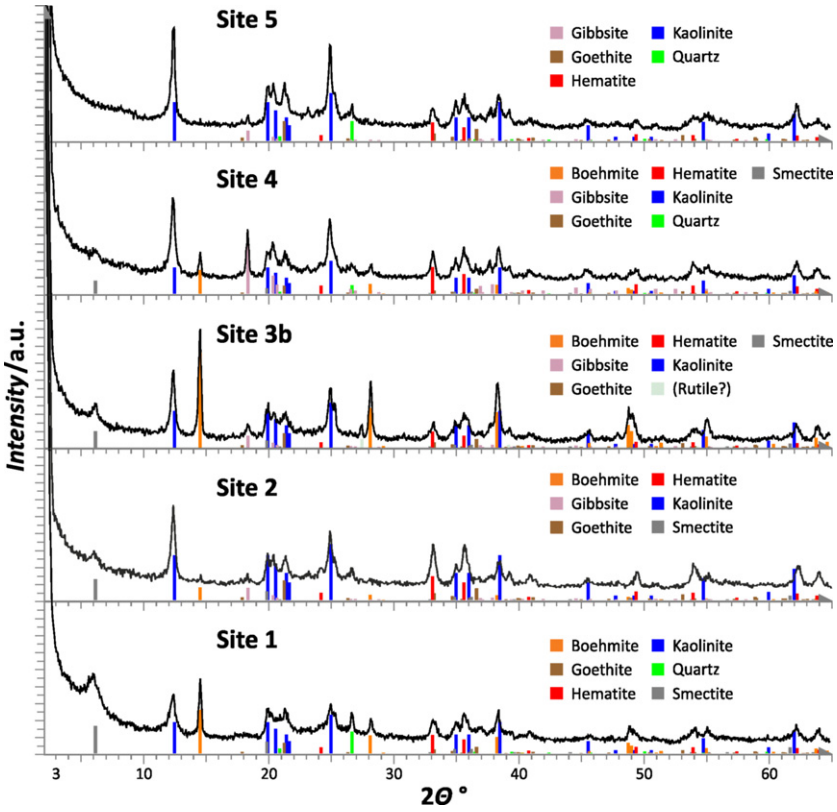


**Fig. 8.** Multiple X-ray diffractogram of the dissolution residues of red calcite samples. The detected minerals are indicated along with their most intense peaks.

All-liquid, all-gas and two-phase primary inclusions were found even within one and the same fluid inclusion assemblage in the red calcite from sites 1 and 3b. In the two-phase (L-V) inclusions the phase ratio is changing from 60:40 to 95:5 (L:V). Number of the phases and the phase ratio are independent from the size of the inclusions in these cases. Most of the primary inclusions in the samples from site 4 are all-liquid, but some of the larger ones (approximately 5% of the total) are of two phases: liquid and vapour. The phase ratio (L:V) is around 90:10 to 95:5. The samples from site 5 are similar to the previously mentioned samples; both one-phase and two-phase primary inclusions were found. The phase ratio is around 80:20 to 95:5.

White calcite from site 3b is characterized by densely packed fluid inclusion-rich laminae. The fact that these inclusions are located along healed microfractures clearly points to their secondary origin (Fig. 10D). The rare primary inclusions are difficult to distinguish from the abundant secondary ones.

To determine the salinity of the fluid entrapped in the primary inclusions cryoscopic measurements were carried out on all-liquid and two-phase inclusions. In the case of the all-liquid inclusions, artificial stretching (*sensu* Goldstein & Reynolds 1994) was necessary to nucleate bubbles to be able to observe freezing and final melting temperature of the fluid. One freezing–heating cycle, down to 40°C, was usually enough to generate bubbles in the one-phase (L) inclusions. Salinity, calculated from the final melting temperature values (based on the equation of Bodnar 1993) of the ice varies between 0 and 0.17 NaCl equ. w% in the case of sites 1 and 3b. Salinity of the primary inclusions of red calcites from sites 4 and 5 is 0 NaCl equ. w%, *i.e.* freshwater (Fig. 11).

## Stable isotope study

Stable oxygen and carbon isotope studies were carried out on red calcite, host rock and transparent calcite samples. Data of this study are compared with the previously published stable isotope data of red calcites from the same localities (Demény *et al.* 1997; Gál-Sólymos 2007). Stable isotope values of vein-filling red calcite in this study for $\delta^{18}O$ are −6.07 to −4.47 ‰ (−2.57 ‰ is an outstanding value measured on highly corroded, therefore probably diagenetically altered red calcite) and for $\delta^{13}C$ are −11.71 to −3.55 ‰ (Table 2, Fig. 12). The observed $\delta^{18}O$ range is very narrow, whilst the $\delta^{13}C$ data cover a wide interval. Stable isotope values of bulk samples from the host rocks are −11.02 to −0.72 ‰ for $\delta^{18}O$ and −1.84 to 2.72 ‰ for $\delta^{13}C$. The reason for this wide interval is probably the different age of the rocks, hosting red calcite, but the influence of diagenesis (e.g. dissolution/recrystallization/

**Table 1** List of solid inclusions detected in the HCl-insoluble residue of the red calcite samples from the different localities.

| | Site 1 | | Site 2 | | Site 3b | | Site 4 | | Site 5 | |
|---|---|---|---|---|---|---|---|---|---|---|
| | XRPD | SEM | XRPD | SEM | XRPD | SEM | XRPD | SEM | XRPD | SEM |
| Gibbsite | | + | + | | + | | + | | + | |
| Boehmite | + | | + | | + | | + | | | |
| Diaspore | | | | | | | | | | |
| Illite | | + | | + | | + | | | | |
| Kaolinite group | + | + | + | | + | + | + | + | + | + |
| Smectite group | + | | + | | + | + | + | | | |
| Hematite | + | + | + | | + | + | + | + | + | + |
| Goethite | + | | + | | + | | + | + | + | |
| Lepidocrocite | | | | | | | | | | |
| Pyrite | | + | | | | + | | + | | |
| Quartz | + | + | | | + | | + | | + | + |
| Garnet | | + | | | | + | | | | |
| K-feldspar | | + | | | | | | | | + |
| Plagioclase | | + | | | | | | | | |
| Kyanite | | + | | | | | | | | |
| Amphibole | | | | + | | | | | | + |
| Pyroxene | | + | | +? | | | | | | +? |
| Mica | | + | | + | | | | | | |
| Epidote | | | | | | | | | | +? |
| Barite | | | | | | + | | | | + |
| Dolomite | | | | | | + | | | | |
| Ilmenite | | | | | | + | | | | + |
| Zircon | | | | | | + | | | | + |
| Rutile (Ti-oxide) | | + | | + | + | + | | | | |
| Apatite | | + | | | | | | | | |
| Monacite | | | | | | + | | | | |
| Cr-spinel | | | | + | | + | | | | + |

XRPD, X-ray powder diffraction, SEM, Scanning electron microscopy.

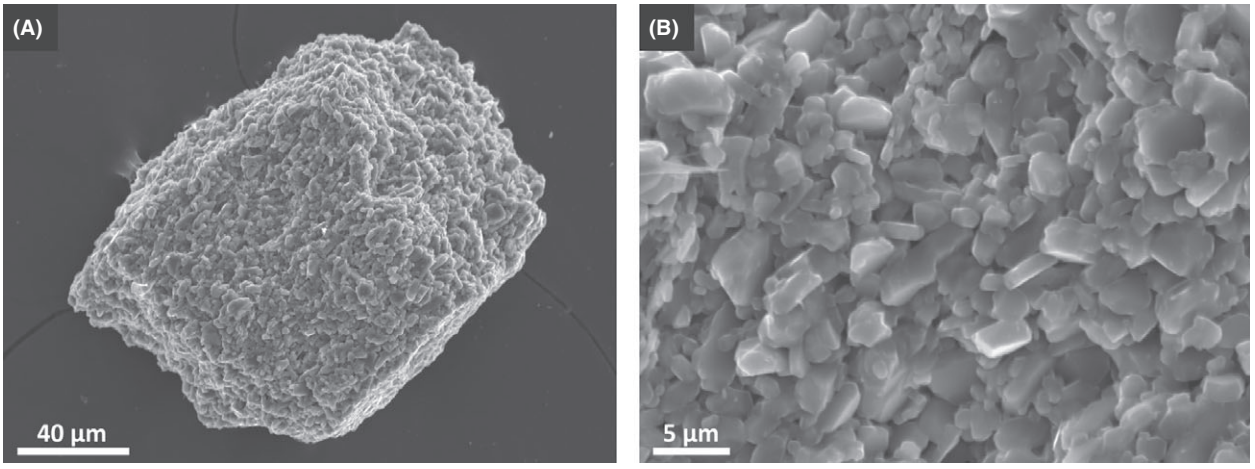


**Fig. 9.** (A) SEM-SE image of an AlOOH aggregate grain from the dissolution residue of the red calcite from site 1; (B) The tabular habit AlOOH crystals, higher magnification image of the grain on figure (A).

cementation) on the stable isotope values cannot be discarded either. Stable isotope values of pink calcite cement found in Rudistid shells of Campanian–Maastrichtian platform limestone (unconformably covering the Aptian limestone at site 1) overlap with the range of the red calcite (−6.32 and −5.83 for $\delta^{18}O$ and −7.74 and −5.28 for $\delta^{13}C$). To assess the stable isotope composition of the Eocene seawater, *Ostrea* shell fragments were measured from the Eocene limestone. Stable isotope values of the bioclast are −2.62 ‰ for $\delta^{18}O$ and 1.33 ‰ for $\delta^{13}C$. Stable isotope composition of young calcite (post-red calcite, *i.e.* the calcite cross-cutting both the host rock of the red calcite and the overlying sediments) is displayed on the diagram for comparison. Yellowish calcites from site 3b

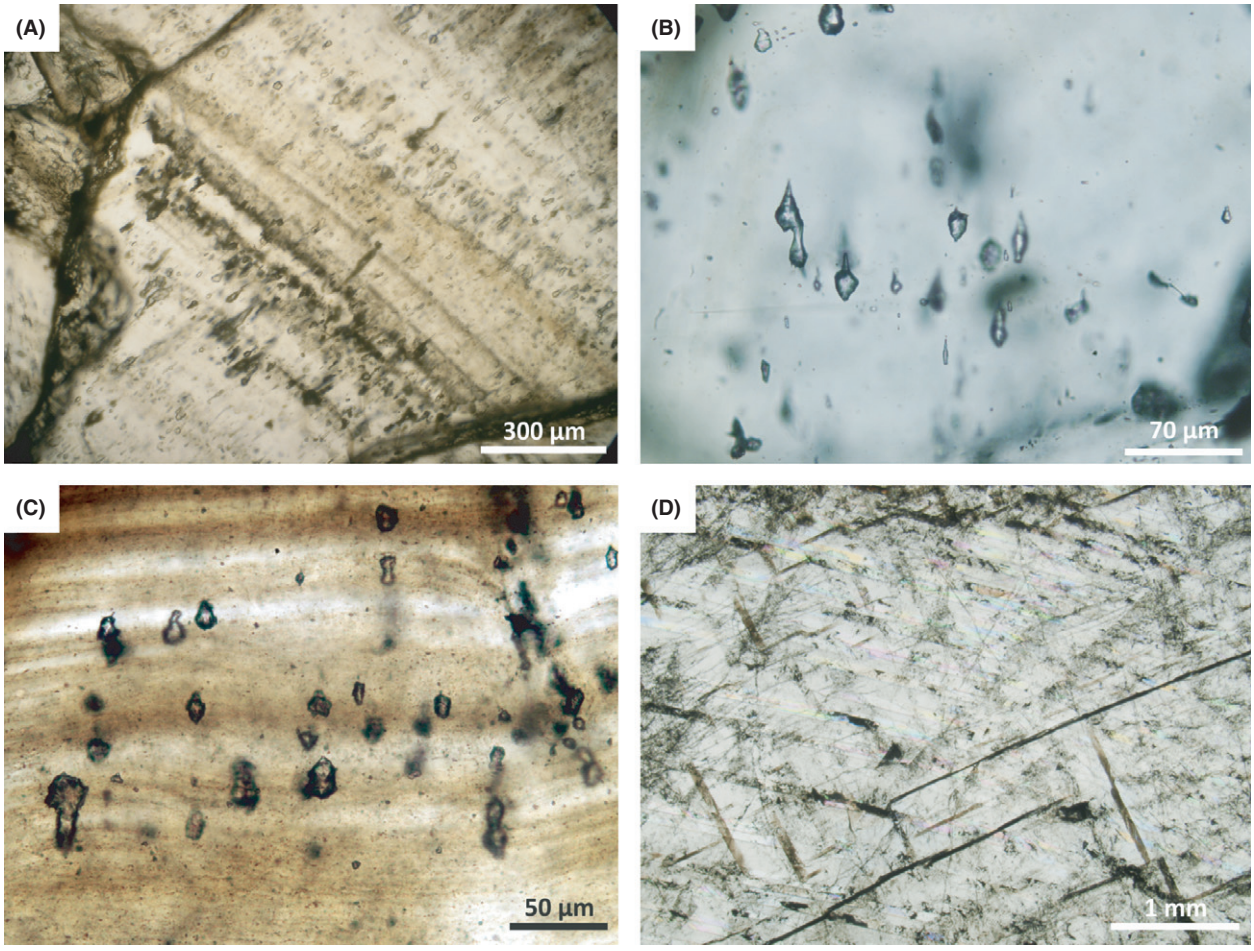


**Fig. 10.** (A) Elongate primary fluid inclusions along the solid inclusion rich laminae of red calcite from site 1; (B) All-liquid and liquid-vapour primary spike-shaped inclusions in red calcite from site 3b; (C) Solid inclusion rich laminae of red calcite from site 4, hosts all-liquid, two-phase (L-V), and all-gas (dark) inclusions; (D) White calcite from site 3b contains secondary fluid inclusions along healed micro-fractures and cleavage planes.

represent a narrow $\delta^{18}O$ isotope (−12.78 to −11.47 ‰) interval and a rather narrow $\delta^{13}C$ isotope range (−7.04 to −4.11 ‰), whilst yellow, white and transparent calcites from site 4 show wide $\delta^{18}O$ isotope range (−14.34 to −8.37 ‰) and the values for $\delta^{13}C$ are between −2.82 and 0.25 ‰. These young calcites are always more depleted in $\delta^{18}O$ than red calcites.

## DISCUSSION

### Diagenetic realm of red calcite precipitation

The corroded, undulatory boundaries of red calcite filled fractures and cavities point to dissolution prior to calcite precipitation. The lack of divalent iron content suggests oxidizing conditions during precipitation. Salinity of primary fluid inclusions is around 0 NaCl w%, suggesting that the parent fluid of the calcite was meteoric water. This is further confirmed by the stable isotope data of the red calcite, which all follow the 'meteoric water line' defined by Lohmann (1988). Spike shape of the primary fluid inclusions, indicating the growth orientation, is typical for speleothems (Goldstein 1990; Csoma *et al.* 2006). Based on the listed observations red calcite, from each studied locality, is considered to be a meteoric precipitate in karst environment. According to the obvious meteoric character of the red calcite, here we suggest to abandon the previously proposed magmatic-hydrothermal model (Demény 1992; Demény *et al.* 1997; Gál-Sólymos *et al.* 2008). High homogenization temperatures (approximately 100–180°C), measured on the primary fluid inclusions by previous authors (Gatter 1984; Demény *et al.* 1997) could be the result of either (i) postentrapment changes in the inclusions (such as stretching and/or leaking); or (ii) heterogeneous entrapment in the vadose zone might have resulted in two-phase inclusions, but in this particular case the measured temperatures

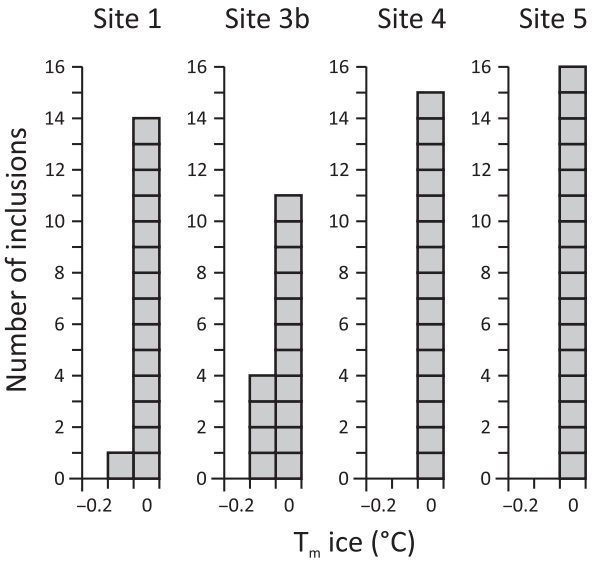


**Fig. 11.** Histogram of final melting temperature of ice ($T_m$) measured in primary aqueous inclusions of red calcites from the different localities.

should not be considered as estimates for the entrapment temperature (*cf.* Goldstein & Reynolds 1994).

Karstic environment for the formation of the red calcite is further confirmed by the facts that red calcite includes traces of bauxite; it exhibits flowstone morphology and micro-fabric; and it is associated with karstic features, such as calcite-cemented bauxitic clay, pisoidal bauxite and collapse breccias. The presence of dissolution-enhanced fractures cemented by red calcite is also characteristic for the meteoric karst. However, these phenomena obviously represent different levels of the paleokarst system, namely the phreatic, the epiphreatic (water-table fluctuation zone) and the vadose zones (James & Choquette 1988, Palmer 2009). Both vadose and phreatic origin of red calcite is suggested by the following field observations. Vadose zone is commonly characterized by vertical shafts and meanders, while phreatic conduits usually have elliptical and often constant cross-section in all dimensions (Jeannin *et al.* 2007). At the investigated localities the extent of the cavities is vertical or isometric and meandering habit is also very common; therefore they rather represent the vadose zone. Neighbouring vadose passages are commonly independent and roughly parallel to one another (Palmer 2009), that is very characteristic for site 3b (Fig. 4B). At this place, red calcite flowstone was observed in the very same horizon as fractures filled with similar laminated red calcite. Here, vadose flowstone-precipitation might have been so pronounced, that the calcite completely occluded the fracture. Those cavities filled up with homogenous (nonlaminar) red coarse-crystalline calcite could represent either an advanced phase of cementation in the vadose zone or they might be phreatic zone precipitates.

Considering field-evidence and micropetrographic observations, the primary fluid inclusion assemblage may point to the previously described two different entrapment scenarios. First possibility is that the formation of the calcite took place in the phreatic zone, below 50°C. This means that at the time of entrapment all primary inclusions were all-liquid. However, these inclusions later (during burial) could have suffered thermal reequilibration (*sensu* Goldstein & Reynolds 1994). Due to the increasing external pressure, overpressure can develop inside the inclusion, which may cause leakage and refilling or stretching. This process is rather common in such 'fragile' minerals as calcite (Goldstein & Reynolds 1994). The 'degree' of reequilibration is also controlled by the size, shape and orientation of the individual inclusions. Larger inclusions are more unstable, which explains that larger two-phase inclusions may be observed next to smaller all-liquid inclusions.

The other scenario is that the calcite precipitated in the vadose zone. In this case, the primary inclusions should contain liquid and vapour (air) phases with variable phase ratios. Two differences from the previously mentioned case are that the liquid–vapour ratio would be independent from the size of these inclusions, and that the vapour phase in the inclusions trapped in the vadose zone would be air, not $H_2O$-vapour.

In the samples from sites 1, 3b and 4 the variable L:V phase ratio of the inclusions supports cementation in the vadose zone for the analysed samples. On the other hand, in samples collected from site 5, the larger inclusions are always of two-phase, suggesting precipitation in the phreatic zone and later reequilibration. It proves that both phreatic and vadose cementation occurred in the case of the red calcite.

### Origin of the solid inclusions

The HCl-insoluble dissolution residue of the red calcite from each locality contains hematite, boehmite and gibbsite, which are common bauxite minerals. The observed detrital mineral assemblage (monazite, xenotime, zircon, apatite, Cr-spinel) is very similar to that of the bauxites of the TR (Mindszenty *et al.* 1991). The presence of these minerals as solid inclusions, suggests that at the time of the precipitation of calcite, not (completely) lithified bauxite was present nearby. However, this model does not necessarily require finding bauxite together with red calcite in each outcrop, for the following two reasons: (i) bauxite, together with some of the red calcite, might have been eroded. (ii) red calcite and bauxite might have formed at different segments and/or levels of the same karst-system, since topographic differences may induce fluids to migrate even for distances of several kilometres, developing significant groundwater systems (Tóth 2009).

**Table 2** Relation between $\delta^{18}O$ (V-PDB) and $\delta^{13}C$ (V-PDB) for samples of red calcite, young calcite and host rock from the different localities.

| Sample description | Locality | $\delta^{18}O$ (V-PDB) | $\delta^{13}C$ (V-PDB) | Sample type |
|---|---|---|---|---|
| Pale zone of laminted red calcite | Site 1 | −5.03 | −5.19 | Microdrilled |
| Dark red zone of laminated red calcite | Site 1 | −4.86 | −3.55 | Microdrilled |
| Pale brown calcite | Site 1 | −5.27 | −8.88 | Microdrilled |
| Yellow calcite | Site 1 | −5.31 | −8.16 | Microdrilled |
| Lower Cretaceous limestone | Site 1 | −2.95 | 0.83 | Bulk |
| Upper Cretaceous limestone | Site 1 | −4.16 | −1.84 | Bulk |
| Pink calcite filling biomold in Upper Cretaceous limestone | Site 1 | −5.83 | −7.74 | Microdrilled |
| Pink calcite filling biomold in Upper Cretaceous limestone | Site 1 | −6.32 | −5.28 | Microdrilled |
| Pale zone of laminted red calcite | Site 2 | −4,97 | −5,57 | Microdrilled |
| Dark red zone of laminated red calcite | Site 2 | −5,62 | −5,16 | Microdrilled |
| Red calcite | Site 2 | −6,03 | −7,54 | Microdrilled |
| Pale zone of laminted red calcite | Site 3b | −5.44 | −8.52 | Microdrilled |
| Dark red zone of laminated red calcite | Site 3b | −5.16 | −8.93 | Microdrilled |
| Pale zone of laminted flowstone red calcite | Site 3b | −4.75 | −5.87 | Microdrilled |
| Dark red zone of laminated flowstone red calcite | Site 3b | −4.47 | −5.26 | Microdrilled |
| Red calcite | Site 3b | −4.49 | −8.20 | Microdrilled |
| Brown calcite | Site 3b | −5.80 | −9.65 | Microdrilled |
| White calcite | Site 3b | −7.08 | −6.72 | Bulk |
| White calcite | Site 3b | −8.34 | −5.02 | Bulk |
| White calcite | Site 3b | −7.28 | −7.86 | Microdrilled |
| Yellow calcite (under barite) | Site 3b | −11.66 | −6.87 | Microdrilled |
| Yellow calcite (bordered by limonite) | Site 3b | −11.47 | −7.04 | Microdrilled |
| Yellow rhombohedral calcite | Site 3b | −12.78 | −4.11 | Microdrilled |
| Yellow transparent calcite with black inclusions | Site 3b | −12.66 | −6.79 | Microdrilled |
| Transparent rhombohedral calcite | Site 3b | −11.89 | −4.15 | Microdrilled |
| Ostrea from Eocene limestone | Site 3b | −2.62 | 1.33 | Microdrilled |
| Eocene limestone | Site 3b | −4.81 | −0.66 | Bulk |
| Upper Triassic dolomite | Site 3b | −6.65 | 2.72 | Bulk |
| Upper Triassic dolomite | Site 3b | −0.72 | 0.79 | Bulk |
| Red calcite | Site 4 | −6.07 | −11.71 | Microdrilled |
| Upper Triassic dolomite | Site 4 | −11.02 | −1.16 | Microdrilled |
| Young transparent calcite | Site 4 | −8.37 | 0.13 | Microdrilled |
| Yellow calcite from the Oligocene sandstone | Site 4 | −13.85 | 0.25 | Microdrilled |
| Yellow calcite overgrown to red calcite | Site 4 | −12.29 | −2.82 | Microdrilled |
| Young white to yellow calcite | Site 4 | −14.34 | −1.18 | Microdrilled |
| White zone of laminated red calcite | Site 5 | −4.80 | −10.59 | Microdrilled |
| Red zone of laminated red calcite | Site 5 | −4.91 | −9.13 | Microdrilled |
| Red, dissolved calcite | Site 5 | −2.57 | −9.18 | Microdrilled |
| Yellow calcite | Site 5 | −4.92 | −9.38 | Microdrilled |
| Yellow calcite | Site 5 | −4.92 | −10.42 | Microdrilled |

Alternation of white and red bands in the calcite, due to the uneven distribution of the solid inclusions, implies that periodic processes could have influenced the precipitation. The periodicity might have been seasonal. In this case, higher rates of rainfall resulted in increased and rapid infiltration in the karstic aquifer and therefore more dilute water with higher amounts of transported particles (Frisia *et al.* 2000) leading to the precipitation of red, solid-inclusion-rich zones of calcite, while limpid, solid-inclusion-poor zones were probably precipitated at times of lower rates of rainfall (cf. Pronk *et al.* 2008).

Iron-oxide inclusions giving red to brown colour to breccia-cementing calcite in the caves of the Black Hills, US, originated from the oxidation of pyrite of the host dolomite, by downward percolating groundwater (Palmer & Palmer 2008). Such pyrite, formed as a by-product of sulphate-reduction (Palmer & Palmer 2008), was not observed in the red calcites of the TR. However, oxidation of detrital pyrite transported into the bauxite, could have resulted in the formation of iron-oxides in this case, too.

## Morphology of the calcite

Morphology of the red calcite could have been influenced by several factors, such as temperature, precipitation rate and style, the velocity of the flowing water, the amount of transported particles and the variation of all these factors through time.

The presence of dripstone and flowstone structures at site 3a and b indicate precipitation from dripping and flowing waters. Such speleothems are usually composed of calcite, grow distinct layers and are composed of elongate (rod or needle-shaped) crystals arranged perpendicular to the growth surface (Palmer 2009).

Large crystals (such as those from sites 2, 3b and 4) suggest that the number of nuclei was relatively small

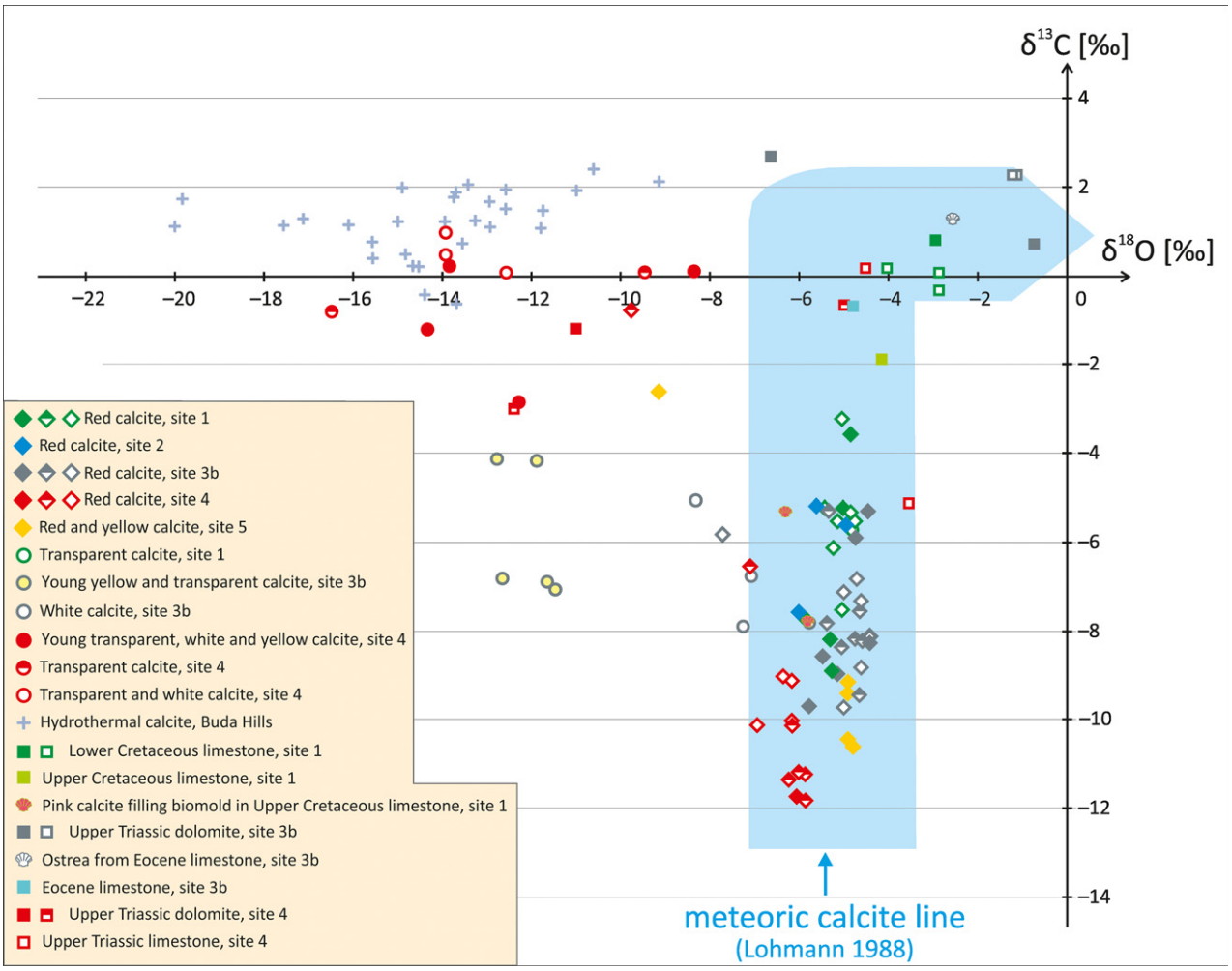


**Fig. 12.** Relationship between $\delta^{18}O$ (V-PDB) and $\delta^{13}C$ (V-PDB) for red calcite, young calcite and host rock from the different localities (filled symbols are data of this study; half-filled symbols: data from Gál-Sólymos *et al.* 2008; empty symbols: data from Demény *et al.* 1997; data of the Miocene (hydrothermal) calcite are from Poros *et al.* 2013).

and/or they formed relatively slowly, both implying that the parent fluid was only slightly supersaturated with respect to calcite (Fairchild *et al.* 2007; Palmer 2009; Frisia & Borsato 2010). Microcrystalline fabric could develop as a result of differing orientation of some crystallites with respect to their substrate, indicating high disturbance of the system related to flow variability and periodic input of growth inhibitors. It forms at the same supersaturation conditions as columnar fabric (Fairchild *et al.* 2007). A decrease in solution supply, and therefore increased supersaturation, could have caused precipitation of fibrous crystals (e.g. site 3b and 4). The process behind the decrease is supposedly the change in the mass-transfer of solutions from gravitational flow to a gravitation-influenced capillary thin-film flow (according to Self & Hill 2003). Fibrous morphology suggests that the crystals might have been primarily aragonitic, later recrystallized to calcite. Aragonite formation has been ascribed to an increase in the Mg concentration of the parent fluid (Harmon *et al.* 1983). At sites 3b and 4, the dolomitic host rock could have provided the Mg for this process. This is supported by the observation of Frisia *et al.* (2002), who found that those passages of Grotte de Clamouse (France) cut in dedolomite host aragonite speleothems, while in limestone passages aragonite was not found.

Solid inclusions transported onto the growth surface of the calcite might have terminated the growth resulting in the nucleation of new crystals.

### Process of precipitation

Fluid flow in the conduits of karstic aquifers is known to be rapid (often >100 m $h^{-1}$) and commonly turbulent (Gold-

scheider *et al.* 2007). All the samples related to the red calcite filled fractures and cavities, such as paleokarst breccias, bauxite ooids, fine-grained bauxitic mud, were cemented by calcite. This suggests that the flux, of fluid from which the calcite precipitated, should have been high enough to reach almost every cavity, whether it was filled with sediment, or not. If sediment was there, either as a matrix of collapse breccia or as an infiltrated fine grained material, it became cemented by calcite. Breccia cemented by red calcite and cross-cut by a red calcite vein found at site 4 clearly indicates that the process was not instantaneous, since the breccia should have been already lithified when the fracture cut it through and red calcite precipitated in it.

Significant amounts of speleothem-type red calcite, found in the TR associated with the bauxitic unconformities, is in good accordance with the fact that tropical climate is characterized by higher mean soil $pCO_2$ at higher mean annual temperatures (Harmon *et al.* 1975) and by positive relationship between growing season soil $pCO_2$ and mean annual evapotranspiration (Brook *et al.* 1983). Waters with higher $pCO_2$ can carry more dissolved carbonate and hence they can precipitate more carbonate on degassing (Fairchild *et al.* 2007).

Dedolomitization, observed along red calcite filled fractures in dolomite host rock, needs to be discussed in detail. This process is a replacement of dolomite by calcite (Goldberg 1967), and it is often ascribed to meteoric fluids (De Groot 1967; Lee & Harwood 1989; Arenas *et al.* 1999; Ronchi *et al.* 2004; Nader *et al.* 2008; Rameil 2008). Some case studies indicate that sulphate-rich solutions are more efficient in dedolomitization as a result of their higher Ca-content, maintaining low $Mg^{2+}/Ca^{2+}$ ratio in solution (Raines & Dewers 1997; Fu *et al.* 2008; Košir *et al.* 2013). However, this explanation is not applicable in the case of the TR, since there are no significant evaporite deposits known in the vicinity of the red calcite occurrences. An experimental study of dedolomitization shows that to be effective, it requires a high rate of water flow, a partial pressure of carbon dioxide much lower than 0.5 atm, and temperatures not higher than 50°C (De Groot 1967); conditions apparently provided by the karstic environment. It was shown by a reactive transport modelling study (Ayora *et al.* 1998) that if the infiltrating water is undersaturated with respect to calcite, calcite dissolution post-dates dedolomitization. This process could be responsible for the widening of open fractures, where the dissolution front follows the dedolomitization front into the dolomite matrix. Dedolomitization observed at sites 3b, 4 and 5 can be described by this process. This interpretation is further supported by other known occurrences in the TR of similar red calcites associated with dedolomitization caused by interaction with karst waters during a pre-Late Eocene subaerial exposure period (Tóth & Tóth-Gecse 1981; Poros *et al.* 2013).

### Age of the red calcite

After the deposition of the oldest rock (the Upper Triassic dolomite) hosting red calcite, and before the youngest (Oligocene) cover rock of the calcite precipitates, four subaerial periods are known in the geological history of the Transdanubian Range: the Albian, the Senonian (Turonian?–Santonian), the Paleocene–Eocene and the early Oligocene (Fig. 2). Bauxite formation was associated to all of them (Mindszenty *et al.* 1991).

Karst-related red calcites from the different localities represent different stratigraphic intervals. This interval is the narrowest at site 1, where the Campanian–Maastrichtian limestone covers the red calcite hosting Aptian limestone. The fact that red calcite fragments were found at the base of the Campanian–Maastrichtian limestone, suggest that the red calcite should have formed here sometime during the Aptian to Campanian apparent stratigraphic gap. The even larger apparent gap, represented by red calcite from site 3b (Late Triassic to Middle Eocene), and sites 4 and 5 (Late Triassic to Early Oligocene) does not allow to specify the age of these deposits within the given time period. The observed Eocene fossils in the sediment covering the surface of a red calcite dripstone at site 3a indicate that the remaining space in the cave in which the calcite formed was ultimately filled by Eocene sediments. The above observation suggests that red calcite formed right before the onset of the Eocene sedimentation. At site 4 and 5, the overlying siliciclastic sediment, which contains fragments of the red calcite, gives the minimum age for the calcite as late Early Oligocene at these outcrops.

Fractures filled with red calcite may also provide information about the age of the calcite by comparing the orientation of the fracture sets to the stress field evolution of the TR (Fodor 2008, 2010). Since dissolution had affected the walls of the fractures, the kinematics of the individual fractures/faults was not possible to determine. However, by looking at the tectonic evolution of the wider surroundings, it is possible to link the red calcite cemented structural elements to certain tectonic phases. The proposed age of the investigated fracture sets would give the maximum age for the precipitation of the calcite. Calcite-cemented fractures might belong to several deformation phases which span from the Albian to the early Eocene. The evolution of the fault pattern and stress field is not uniform throughout the TR but shows regional variations and the phases and subphases are not well separated in time. The oldest possible age, the early Albian, can be excluded for the formation of all calcite occurrences, because the orientation of the fractures cemented by red calcite does not fit into the stress field established for that period (D2b and D2c on Fig. 6B). Considering this, a possible relationship to the Albian bauxite horizon can be excluded.

The dominant map-scale structures, the NE–SW trending folds and reverse faults of the TR, belong to the D3 phase of NW–SE compression (Fig. 6B), and could have occurred between Albian and Coniacian times (113–86 Ma). Some NW–SE trending fractures measured at sites 2a, 3a, 3c might belong to this phase, although alternative interpretation (phase D6) is possible. This long phase has local spatial variation within the Vértes Hills, where the compression ($\sigma_1$ axis) was oriented more towards N–S. This D3d phase probably occurred between 90 and 86 Ma (Fodor 2008). Several calcite infills occur along this fault set in the Vértes Hills (sites 2a, 2d).

There is only limited information available about the fracture sets and poor time constraints for the stress field between 86 and 48 Ma. Fodor (2010) estimated NE–SW extension for the late Cretaceous (D4 phase) using a limited data set. The D5 strike-slip phase with ENE–WSW compression seems to post-date the Cretaceous and predate the mid-Eocene (Fig. 6B). Fractures being parallel to this compressional direction probably belong to this phase at site 2b. Finally, the fracture pattern changed to strike-slip type in the Middle Eocene (phase D6) and kept this style throughout the Palaeogene.

Measurements revealed a new fracture set of NNE–SSW to NE–SW orientations that is cemented by red calcite at sites 1 and 3b (Fig. 6A). These fractures are younger than the D3 phase, because they occur with steep orientation in already tilted Mesozoic layers; at site 1 they cut steep to subvertical Aptian beds. These directions are between the compressional direction of D4 and D5 phases, therefore they can be assigned to the D4/D5 event. The age may be late Cretaceous (90–65 Ma), but is poorly constrained. Kercsmár (2004, 2008) associated the formation of NE–SW striking, red calcite-hosting fractures to a local flexural extension on the hinge of an anticline at sites 3a and 3b. In this scenario the fractures might belong either to D3 or to D4 phases. Even if we accept this later scenario, the NE–SW trending fractures remain poorly dated with no structural evidence to document the fold-hinge-parallel position of the fractures.

At sites 2 and 3, the age of the overlying beds is Middle Eocene, while at sites 4 and 5 the overlying bed is Oligocene, and only Eocene and Oligocene bauxites are known in the area (Mindszenty *et al.* 1991). This would imply that the erosion also reached the associated karst system, including the red calcite speleothems. Therefore, it is more likely that the red-calcite is associated to the Eocene or Oligocene bauxite horizon, and the formation of the fractures is related to the Middle Eocene–Oligocene stress field (phase D6) at sites 2a, 3a, 3c. Cr-spinel, found in the calcite from sites 2, 3b and 5, known from the Eocene bauxite horizon (Mindszenty *et al.* 1991), further confirms the above theory.

### Hydrogeological aspect

Meteoric fluids are known to transport solid particles not only down to the water table but also beyond. The flow is driven by topographic differences, forcing the water to move according to a hierarchically nested flow system (Tóth 2009). At the same time in a carbonate rock mass the flow pattern is highly influenced also by fractures, since water moves faster along conduits in the karst (Palmer 2009).

Vertical shafts are abundant at sites 1, 3b and 4. They host large amounts of red calcite speleothems. This implies that, at one and the same place, first dissolution and then precipitation took place. Erosion of the overlying sediments above the Cretaceous and Triassic carbonates must have resulted in a relatively bare surface. In this phase the karst was unconfined in which the diffuse flow could have been more pronounced than the concentrated one (Fig. 13A). As the karst evolved, this ratio changed, focussing the flow into fractures that developed into vertical conduits (Fig. 13B,C). Simultaneously, under the favourable climatic conditions, bauxite started to form on the surface. The evolution of the topographic depressions, in which bauxite accumulates, usually goes hand in hand with the accumulation of the bauxitic material (Bárdossy 1989). Therefore, one may expect larger cavities below bauxite deposits, than below bauxite-free areas in the karst (Bárdossy 1989). Bauxite particles were transported into the karst by the downward moving water (Fig. 13D). Precipitation of calcite was mostly triggered by outgassing of $CO_2$ and/or evaporation as water has reached open cavities. As soon as the $pCO_2$ of water exceeds that of the cave, evaporation becomes the predominant process (Gonzalez & Lohmann 1988).

Rudistid bivalve-filling pink calcite, from the Campanian–Maastrichtian limestone, has similar $\delta^{13}C$ values than those of the red calcite from site 1; however; $\delta^{18}O$ values of the biomold calcite are slightly higher than that of the red calcite from the same place. This implies that they precipitated from the same fluid system, but at different times and at different levels of the karst (Fig. 14). The top of the exposed Aptian limestone was a recharge area at the place and time of red calcite formation (*i.e.* sometime between the late Aptian and the Late Campanian). The red calcites precipitated near the surface from low-temperature (below 50°C) fluids. As a result of transgression, Rudistid reefs started to develop on the shallow shelf. Meteoric water circulated from the mainland into the reef body, precipitating meteoric calcite cement (Mindszenty *et al.* 2001). At this time the former site of red calcite cementation moved to a 'discharge' position, where meteoric fluids had slightly elevated temperature, as they were at the end of a longer route. This could be reflected in the $\delta^{18}O$ values of the biomold-filling pink calcite being slightly higher, than that of the red calcites. In the same time pink colour

suggests lower amounts of hematite inclusions, than in the case of the red calcites. The above described process implies that in the case of site 1 the red calcite precipitated slightly before the onset of the reef formation during the late Campanian.

### Young calcite-barite vein generation

Stable isotope values of the transparent, yellow and white calcites from site 3b and 4, previously interpreted to be relatives of the red calcites, (data from Demény *et al.* 1997 and Gál-Sólymos *et al.* 2008) are very similar to those of the Miocene vein-filling calcite generation known from neighbouring parts of the Buda Hills (Poros *et al.* 2012). Therefore, the calcite-barite veins from the studied locations are rather related to the same Miocene regional fluid migration event, which also created the calcite-barite veins of the Buda Hills.

## CONCLUSIONS

Field observations and petrographic data provided evidence for the red calcite being a speleothem that formed in a karst system below a bauxitic unconformity. Stable oxygen and carbon isotope data, which all follow the meteoric line, and approximately 0 NaCl equ. w% salinity of the fluids in primary inclusions support meteoric origin. Flowstone and dripstone structures observed at one of the localities correspond to the formation in the vadose zone. Enclosed particles, now present as solid inclusions in the calcite, were derived from the bauxite that once extensively covered the exposed surface of the karst. Hematite gives the red colour to the calcite. The colour banding in the calcite indicates that the bauxite supply was periodic (probably seasonal).

Stratigraphic considerations, supported by structural geologic observations, allowed the establishment of only two possible intervals in which red calcite could form. Red calcite at site 1 was most probably formed in late Cretaceous (Campanian?) times and it might be associated to the 'Senonian' bauxite horizon. Calcite at the other studied locations is associated with the Eocene bauxite horizon that suggests Eocene age in these cases.

Since good drainage is needed for the formation of thick bauxite deposits, it can be expected that red calcite speleothems would develop at those places where bauxite had long enough time to form and the karst was mature. Thus, red calcite occurrence could provide good evidence on bauxite, which existed at the overlying unconformity. Therefore, presence or absence of red calcite could be used as distinguishing criteria between karst episodes with or without bauxite formation. Karst systems with extensive bauxite blanket refer to the mature stage of karstification under humid climate. In the case of a shorter subaerial exposure period, with no bauxite formation associated, one would not expect to find red calcite speleothems. Also, since the appearance of this type of red calcite is so unique, it helps to identify paleo-karst systems that might act as hydrocarbon reservoirs, as well, even from limited core data.

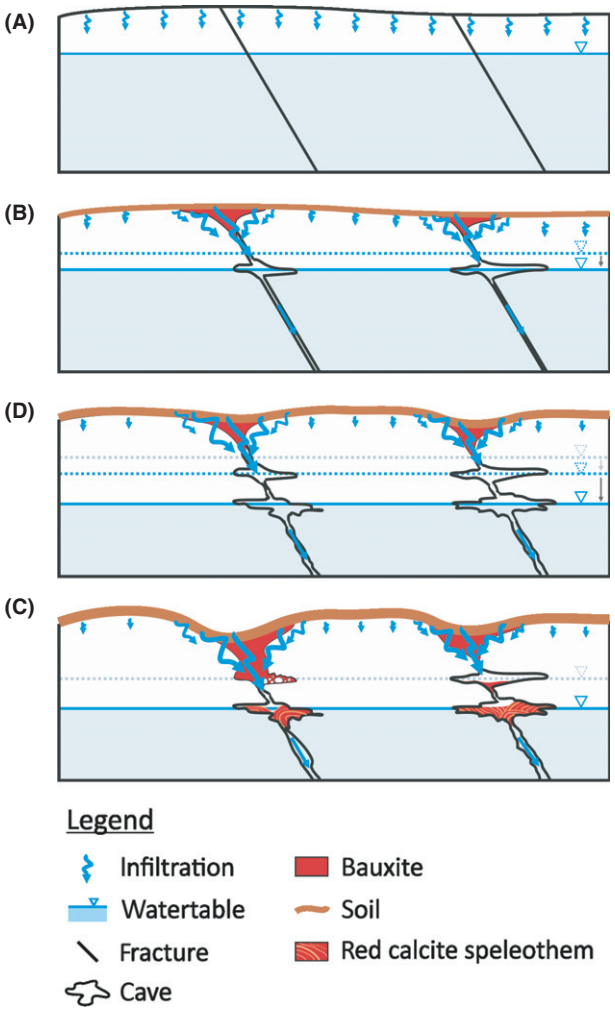


**Fig. 13.** Hydrogeological evolution of the karst; (A) 1st Stage: Diffuse flow is dominant throughout the whole exposed surface. (B) 2nd Stage: Fractures focus the flow, while bauxite starts to accumulate in those areas, where drainage is best. Caves form at the watertable. (C) 3rd Stage: Flow is concentrated along the fractures that develop to conduits. As a result of uplift, watertable moves downward. Caves form at the level of the 'new' watertable. (D) 4th Stage: Particles from the bauxite are washed down into the karst. Red calcite speleothems develop in the watertable caves.

## ACKNOWLEDGEMENTS

First author would like to acknowledge Judit Mádl-Szőnyi, Kinga Hips, János Haas, Csaba Szabó, Márta Berkesi and Georgina Lukoczki for the discussions on the topic. Zsolt Bendő (SEM), Judit Tóth-Király (XRPD) and András Varga (dissolution of the samples) are acknowledged for their help with the instruments and chemical investigations.

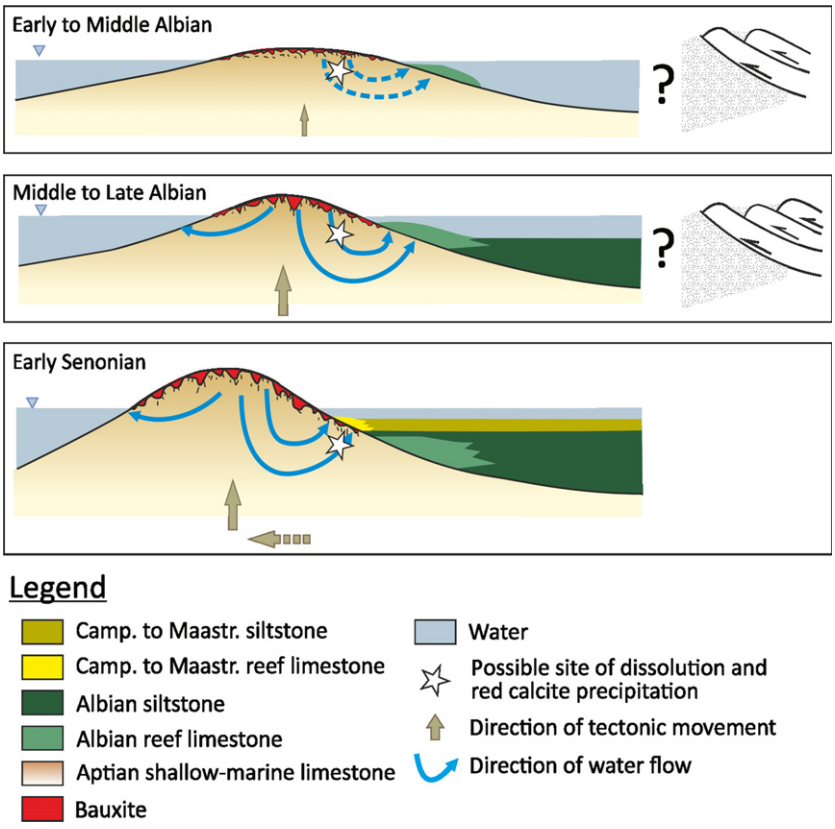


**Fig. 14.** Model for the formation of bauxite in the TR and its relationship to the hydrogeological evolution at site 1 (modified after Mindszenty *et al.* 2001).

Remarks and suggestions of Mark Person, Roman Aubrecht and an anonymous reviewer influenced the final shape of the paper.

## REFERENCES

Angelier J (1984) Tectonic analysis of fault slip data sets. *Journal of Geophysical Research*, **89**, 5835–48.

Arenas C, Alonso-Zarza AM, Pardoa G (1999) Dedolomitization and other early diagenetic processes in Miocene lacustrine deposits, Ebro Basin (Spain). *Sedimentary Geology*, **125**, 23–45.

Ayora C, Taberner C, Saaltink MW, Carrera J (1998) The genesis of dedolomites: a discusion based on reactive transport modeling. *Journal of Hydrology*, **209**, 346–65.

Balásházy L (1979) Detailed tectonic investigations in the N-Vértes and S-Gerecse area. Transdanubia. Hungary (in Hungarian with English abstract). *Általános Földtani Szemle*, **13**, 33–48.

Báldi T, Báldi-Beke M (1985) The evolution of the Hungarian Paleogene basins. *Acta Geologica Hungarica*, **28**, 5–28.

Bárdossy Gy (1989) Bauxites. In: *Paleokarst – A Systematic and Regional Review* (eds Bosák P, Ford DC, Glazek J, Horacek I). Elsevier, New York.

Bertotti G, Picotti V, Bernoulli D, Castellarin A (1993) From rifting to drifting: tectonic evolution of the South-Alpine upper crust from the Triassic to the Early Cretaceous. *Sedimentary Geology*, **86**, 53–76.

Bodnar RJ (1993) Revised equation and table for determining the freezing point depression of $H_2O$-NaCl solutions. *Geochimica et Cosmochemica Acta*., **57**, 683–4.

Bosák P, Ford DC, Glazek J, Horácek I (1989) *Paleokarst. A Systematic and Regional Review*. Elsevier-Academia, Amsterdam-Praha.

Brook GA, Folkoff ME, Box EO (1983) A world model of soil carbon dioxide. *Earth Surface Processes and Landforms*, **8**, 79–88.

Budai T (1989) *Geological Base Sections of Hungary: Balatonfüred, Száka Hill (Füred Limestone Formation)*. Geological Institute of Hungary, Budapest.

Budai T, Császár G, Csillag G, Fodor L, Gál N, Kercsmár Zs, Kordos L, Pálfalvi S, Selmeczi I (2008) *Geology of the Vértes Hills. Explanatory Book to the Geological Map of the Vértes Hills 1:50000*. Geological Institute of Hungary, Budapest.

Combes PJ, Bárdossy Gy (1996) Geodynamics of bauxites in the Tethyan realm. In: *The Ocean Basins and Margins* (ed Nairm AE), pp. 347–65. Plenum Press, New York, London.

Csoma A, Goldstein RH, Pomar L (2006) Pleistocene speleothems of Mallorca: implications for palaeoclimate and carbonate diagenesis in mixing zones. *Sedimentology*, **53**, 213–36.

Csontos L, Nagymarosy A, Horváth F, Kovac M (1992) Tertiary evolution of the Intra-Carpathian area: a model. In: *Geodynamics of Rifting. Volume I.* (ed. Ziegler PA), Tectonophysics, **208**, pp. 221–41.

De Groot K (1967) Experimental dedolomitization. *Journal of Sedimentary Petrology*, **37**, 1216–20.

Demény A (1992) Origin of carbonates in lamprophyres of Hungary: a stable isotope study. *Földtani Közlöny*, **122**, 209–32.

Demény A, Gatter I, Kázmér M (1997) The genesis of Mesozoic red calcite dikes of the Transdanubian Range (Hungary): fluid inclusion thermometry and stable isotope compositions. *Geologica Carpathica*, **48**, 315–23.

Deming D, Nunn JA, Evans DG (1990) Thermal effects of compaction-driven groundwater flow from overthrust belts. *Journal of Geophysical Research*, **95**, 6669–83.

Dickson JAD (1966) Carbonate identification and genesis as revealed by staining. *Journal of Sedimentary Research*, **36**, 491–505.

Fairchild IJ, Frisia S, Borsato A, Tooth A (2007) Speleothems. In: *Geochemical Sediments and Landscapes* (eds Nash DJ, McLaren SJ), pp. 200–45. Blackwell Publishing, Oxford.

Fodor L (2008) Structural Geology. In: *Geology of the Vértes Hills* (eds Budai T, Fodor L), pp. 282–301. Innova-Print Kft, Budapest.

Fodor L (2010) Mesozoic-Cenozoic stress fields and fault patterns in the northwestern part of the Pannonian Basin - methodology and structural analysis (in Hungarian). Doctoral work of the Hungarian Academy of Sciences Budapest, 129.

Fodor L, Kercsmár Z, Sásdi L, Harangi S (2008) Geological arguments against a Late Cretaceous(?) age for the freshwater limestone bodies in the Köves Valley (Vértes Hills, Hungary) (in Hungarian with English abstract). *Földtani Közlöny*, **138**, 181–8.

Frisia S, Borsato A (2010) Karst. In: *Carbonates in Continental Settings – Facies, Environments and Processes* (eds Alonso-Zarza AM, Tanner LH), pp. 269–318. Elsevier, Developments in Sedimentology, Amsterdam, the Netherlands.

Frisia S, Borsato A, Fairchild IJ, McDermott F (2000) Calcite fabrics, growth mechanisms, and environment of formation in speleothems from the Italian Alps and southwestern Ireland. *Journal of Sedimentary Research*, **70**, 1183–96.

Frisia S, Borsato A, Fairchild IJ, McDermott F, Selmo EM (2002) Aragonite-calcite relationships in speleothems (Grotte de Clamouse, France): environment, fabrics and carbonate chemistry. *Journal of Sedimentary Research*, **72**, 687–99.

Fu Q, Qing H, Bergman KM, Yang C (2008) Dedolomitization and calcite cementation in the Middle Devonian Winnipegosis Formation in Central Saskatchewan, Canada. *Sedimentology*, **55**, 1623–42.

Gál-Sólymos K, Gatter I, Józsa S, Korpás L (2008) Genesis of late Cretaceous calcite dykes from the Transdanubium Central Range (in Hungarian with English abstract). *Project Report for the Hungarian Science Foundation*, **20**.

Gatter I (1984) Investigation of embedded fluids in vein fillings and in crusts precipitated from thermal waters on the walls of caves in carbonate rocks (in Hungarian). *Karszt és Barlang*, **1**, 9–18.

Gawlick HJ, Frisch W, Vecsei A, Steiger T, Böhm F (1999) The change from rifting to thrusting in the Northern Calcareous Alps as recorded in Jurassic sediments. *Geologische Rundschau*, **87**, 644–57.

Goldberg M (1967) Supratidal dolomitization and dedolomitization in Jurassic rocks of Hamakhtesh Hagatan, Israel. *Sedimentary Petrology*, **37**, 760–73.

Goldscheider N, Drew D, Worthington D (2007) Introduction. In: *Methods in Karst Hydrogeology* (eds Goldscheider N, Drew D), pp. 1–8. Taylor and Francis Group, London.

Goldstein RH (1990) Petrographic and geochemical evidence for origin of paleospeleothems, New Mexico: implications for the application of fluid inclusions to studies of diagenesis. *Journal of Sedimentary Petrology*, **60**, 282–92.

Goldstein RH, Reynolds TJ (1994) Systematics of fluid inclusions in diagenetic minerals. *SEPM Short Course*, **31**, 199.

Gonzalez LA, Lohmann KC (1988) Mineralogy and composition of spelean carbonates, Carlsbad Caverns, New Mexico. In: *Paleokarst* (eds James NP, Choquette PW). Springer-Verlag, New York.

Gyalog L, Horváth I (eds.) (2004) *Geology of the Velence Hills and the Balatonfő. Explanatory Book of the Geological Map of the Velence Hills (1:25 000) and the Geological Map of Pre-Sarmatian Surface of the Balatonfő-Velence Area (1:100 000)*. Geological Institute of Hungary, Budapest.

Haas J (1983) Senonian cycle in the Transdanubian Central Range. *Acta Geologica Hungarica*, **26**, 21–40.

Haas J (2012) Influence of global, regional and local factors on the genesis of the Jurassic manganese ore formation in the Transdanubian Range, Hungary. *Ore Geology Reviews*, **47**, 77–86.

Haas J, Jocha-Edelény E, Gidai L, Kaiser M, Kretzoi M, Oravecz J (1985) Geology of the Sümeg area. *Geologica Hungarica Series Geologica*, **20**, 365.

Haas J, Kovács S, Krystyn L, Lein R (1995) Significance of Late Permian – Triassic facies zones in terrane reconstructions in the Alpine – North Pannonian domain. *Tectonophysics*, **242**, 19–40.

Haas J, Budai T, Csontos L, Fodor L, Konrád Gy (2010) *Pre-Cenozoic Geological Map of Hungary, 1:500 000.* Geological Institute of Hungary, Budapest.

Harmon RS, White WB, Drake JJ, Hess JW (1975) Regional hydrochemistry of North American carbonate terrains. *Water Resources Research*, **11**, 963–7.

Harmon RS, Atkinson TC, Atkinson JJ (1983) The mineralogy of Castleguard Cave, Columbia Icefields, Alberta, Canada. *Arctic and Alpine Research*, **15**, 503–16.

Horváth F, Cloetingh S (1996) Stress-induced late-stage subsidence anomalies in the Pannonian Basin. *Tectonophysics*, **266**, 287–300.

Horváth I, Ódor L (1984) Alkaline ultrabasic rocks and associated silicocarbonatites in the NE part of the Transdanubian Mts. (Hungary). *Mineralia Slovaca*, **16**, 115–9.

Horváth I, Darida-Tichy M, Ódor L (1983) Magnesitiferous dolomitic carbonatite (beforsite) dyke rock from the Velence Mountains (in Hungarian with English abstract). *Annual Report of the Geological Institute of Hungary*, **1981**, 369–88.

James NP, Choquette PW (1988) *Paleokarst*. Springer-Verlag, New York.

Jeannin P-Y, Groves C, Häuselmann P (2007) Speleological investigations. In: *Methods in Karst Hydrogeology* (eds Goldscheider N, Drew D), pp. 1–8. Taylor and Francis Group, London.

Kázmér M, Kovács S (1985) Permian – Palaeogene paleogeography along the Eastern part of the Insubric - Periadriatic lineament system: evidence for continental escape of the Bakony-Drauzug Unit. *Acta Geologica Hungarica*, **28**, 71–84.

Kercsmár Zs (1995) Paleoenvironmental reconstruction and tectono-sedimentological investigation of the eastern margin of the Tatabánya basin. In: *Department of Paleontology and Department of Applied and Environmental Geology* M.Sc. Thesis, pp. 120, Eötvös Loránd University, Budapest.

Kercsmár Zs (2004) Structural analysis of red calcite veins on Keselő Hill, Tatabánya Basin. *Annual Report of the Geological Institute of Hungary, 2002*, 163–74.

Kercsmár Zs (2008) Budakeszi Picrite Formation and calcite veins. In: *Geology of the Vértes Hills. Explanatory Book to the Geological Map of the Vértes Hills 1:50000.* (eds Budai T *et al.*), pp. 248–50. Geological Institute of Hungary, Budapest.

Korpás L (1981) Oligocene-Lower Miocene Formations of the Transdanubian Central Mountains in Hungary. *Annual Report of the Geological Institute of Hungary*, **64**, 83–140.

Košir A, Martín-Pérez A, Otonicar B (2013) Hypogenically formed dedolomite bodies in the mid-Cretaceous dolomite of

the Povir Formation (Kras, Slovenia). In: *21th International Karstological School "Classical Karst"* Postojna, Slovenia, 86.

Lee MR, Harwood GM (1989) Dolomite calcitization and cement zonation related to uplift of the Raisby Formation (Zechstein carbonate), northeast England. *Sedimentary Geology*, **65**, 285–305.

Lohmann KC (1988) Geochemical patterns of meteoric diagenetic systems and their application to studies of paleokarst. In: *Paleokarst* (eds Choquette PW, James NP), pp. 58–80. Springer-Verlag, New York.

Machel H, Cavell PA (1999) Low-flux, tectonically induced squeegee fluid flow ('hot flash') into the Rocky Mountain Foreland Basin. *Bulletin of Canadian Petroleum Geology*, **47**, 510–33.

Mindszenty A, Gál-Sólymos K, Csordás-Tóth A, Imre I, Felvári Gy, Ruttner AW, Böröczky T, Knauer J (1991) Extraclasts from Cretaceous/Tertiary bauxites of the Transdanubian Central Range and the Northern Calcareous Alps. Preliminary results and tentative geological interpretation. *Ubiläumsschrift 20 Jahre geologische Zusammenarbeit Österreich-Ungarn*, **1**, 309–45.

Mindszenty A, Csoma A, Török Á, Hips K, Hertelendi E (2001) Rudistid limestones, bauxites, paleokarst and geodynamics. The case of the Cretaceous of the Transdanubian Range (in Hungarian with English abstract). *Földtani Közlöny*, **131**, 107–52.

Moore CH (1989) *Carbonate Diagenesis and Porosity*. Elsevier Science, Amsterdam, the Netherlands.

Nader FH, Swennen R, Keppens E (2008) Calcitization/dedolomitization of Jurassic dolostones (Lebanon): results from petrographic and sequential geochemical analyses. *Sedimentology*, **55**, 1467–85.

Pálfalvi S, Fodor L, Kercsmár Zs, Báldi-Beke M, Kollányi K, Less Gy (2006) Sedimentation pattern, tectonic control and basin evolution of the northern Transdanubian Eocene basins (Vértes Hills, central Hungary). In: *Europen Geosciences Union General Assembly*. Geophysical Research Abstracts, Vienna.

Palmer AN (2009) *Cave Geology*. Allen Press, Lawrence, Kansas.

Palmer AN, Palmer MV (2008) Field Guide to the Paleokarst of the southern Black Hills. In: *Karst from Recent to Reservoirs* (eds Sasowsky ID, Feazel CT, Mylroie JE, Palmer AN, Palmer MV), **Special Publication** pp. 189–220. Karst Water Institute, Leesburg, VA.

Poros Zs, Mindszenty A, Molnár F, Pironon J, Győri O, Ronchi P, Szekeres Z (2012) Imprints of hydrocarbon-bearing basinal fluids on a karst system: mineralogical and fluid inclusion studies from the Buda Hills, Hungary. *International Journal of Earth Sciences*, **101**, 429–52.

Poros Zs, Machel H, Mindszenty A, Molnár F (2013) Cryogenic powderization of Triassic dolostones in the Buda Hills, Hungary. *International Journal of Earth Sciences*, **102**, 1513–39.

Pronk M, Goldscheider N, Zopfi J, Zwahlen F (2008) Percolation and particle transport in the unsaturated zone of a karst aquifer. *Groundwater*, **47**, 361–9.

Raines MA, Dewers TA (1997) Dedolomitization as a driving mechanism for karst generation in Permian Blaine Formation, Southwestern Oklahoma, USA. *Carbonates and Evaporites*, **12**, 24–31.

Rameil N (2008) Early diagenetic dolomitization and dedolomitization of Late Jurassic and earliest Cretaceous platform carbonates: a case study from the Jura Mountains (NW Switzerland, E France). *Sedimentary Geology*, **212**, 70–85.

Ratschbacher L, Frisch W, Linzer HG, Merle O (1991) Lateral extrusion in the Eastern Alps, part 2. : structural analysis. *Tectonics*, **10**, 257–71.

Ronchi P, Jadoul F, Savino R (2004) Quaternary dedolomitization along fracture system in a Late Triassic dolomitized platform (western Southern Alps, Italy). *Carbonates and Evaporites*, **19**, 51–66.

Sásdi L (2000) Evolution of the Pilis Karst area. In: Karsztfejlődés Berzsenyi Dániel High School, Szombathely, Hungary, V., 77–93.

Schmid S, Bernoulli D, Fügenschuh B, Matenco L, Schefer S, Schuster R, Tischler M, Ustaszewski K (2008) The Alpine-Carpathian-Dinaridic orogenic system: correlation and evolution of tectonic units. *Swiss Journal of Geosciences*, **101**, 139–83.

Self CA, Hill CA (2003) How speleothems grow: an introduction to the ontogeny of cave minerals. *Journal of Cave and Karst Studies*, **65**, 130–51.

Spötl C, Vennemann TW (2003) Continuous-flow isotope ratio mass spectrometric analysis of carbonate minerals. *Rapid Communications in Mass Spectrometry*, **17**, 1004–6.

Szabó Cs, Kubovics I, Molnár Z (1993) Alkaline lamprophyre and related dyke rocks in the NE Transdanubia, Hungary: the Alcsútdoboz-2 borehole. *Mineralogy and Petrology*, **47**, 27–148.

Taeger H (1909) Geology of the Vértes Mts. *Annales of the Hungarian Royal Geological Institute*, **17**.

Tari G (1994) *Alpine Tectonics of the Pannonian Basin*. Ph.D thesis. pp. 489, Rice University, Texas, USA.

Thompson JFH (1995) *Magmas, Fluids and Ore Deposits*. Mineralogical Association of Canada, Québec.

Tóth J (2009) *Gravitational Systems of Groundwater Flow*. Cambridge University Press, New York.

Tóth Á, Tóth-Gecse É (1981) Dedolomitized dikes in the Upper Triassic basement of the Nagyegyháza Basin (in Hungarian). In: *Annual Report of the Geological Institute of Hungary for 1979*. pp. 181–200. Geological Institute of Hungary, Budapest.